We are grateful to the referees for their time and energy in providing helpful comments and guidance that have improved the manuscript. In this document, we describe how we have addressed the reviewer's comments. Referee comments are shown in black and author responses are shown in blue text. A manuscript with all tracking changes are attached in the end.

Response to the reviewer 1

Review summary:

Lei et al., present a new model that combines a dynamic vegetation model that includes biogeochemistry (YIBs) with a widely used chemical transport model (GEOS-Chem). They run the model offline and with 5 different online conditions. They use model results to validate the model against measurements (particularly gross primary productivity and leaf area index). They explore the effects of building the online model on ozone mixing ratios, ozone deposition, and ozone damaging effects on terrestrial activity (such as gross primary productivity). In general, the global average change in ozone mixing ratios is quite small. However, they do find some notable differences in ozone deposition rates between GC and GC-YIBs, and they find the online model does improve ozone deposition rates when compared to the limited observations that are available. Finally, the utility of the model is demonstrated by their results on the effects of ozone on terrestrial productivity. Using the online model, they find gross primary productivity can decrease up to 15% in certain areas due to the damaging effects of ozone pollution. This study provides a valuable tool for investigating links between the terrestrial biosphere and atmospheric chemistry, which is a critical (and under-studied) research area for predicting the effects of climate change. The authors could improve the manuscript in a couple areas to better communicate their reasoning and clarify concepts to the reader. I recommend the paper for publication after addressing the minor comments summarized below, which should help them accomplish this.

➔ Thank you for your positive evaluations. All the questions and concerns have been carefully answered and the paper has been revised accordingly.

Specific comments:

Section 3.2, particularly lines 305-308. The authors state that the difference in ozone mixing ratios between the Online_All and Online_LAI suggests that "changes in stomatal conductance play the dominant role in regulating surface [O_3]." I am not following this logic and I think they need to better clarify how they are making this connection. The description of the model runs just says Online_All has daily dynamically predicted LAI and hourly predicted stomatal conductance while the Online_LAI has daily dynamically predicted LAI and the original dry deposition scheme. It is not obvious to me how comparing the output of these two model simulations leads to the conclusion they have provided, and this could be better explained.

Response: The configurations of Online_ALL and Online_LAI simulations are the same except for stomatal conductance. Online_ALL simulation uses hourly stomatal conductance simulated by YIBs, which dynamically responds to environmental factors (e.g., temperature, water stress, radiation, CO_2 and so on). However, Online_LAI simulation uses prescribed stomatal conductance, though it uses online-predicted LAI the same as Online_ALL. As a result, the difference between Online_ALL and Online_LAI represents the effects of updated stomatal conductance on surface [O_3]. In revised paper, we changed "the original dry deposition scheme" to "prescribed stomatal conductance" to clarify. (Line 298)

Discussion of Figure 6 and 7: it is unclear what value is added by including figure 6. The figure shows the different land types in the original GC dry deposition scheme where different land types are prescribed fixed parameters for stomatal conductance. The online model is different because it calculates stomatal conductance based on photo-synthesis and environmental forcings (L. 332-333). Then they show that dry deposition comparisons between the original and online model vary by biome type in

Figure 7. This would be expected simply knowing the original model uses prescribed parameters based on land type while the online model calculates stomatal conductance! The map shown in Figure 6 does not provide any additional useful information. It might be more helpful to describe in more detail how the fixed parameters in the original GC model were developed. That would be more useful than the map of different land types.

Response: The main purpose of Fig. 6 is to show the location and deposition land type of sites (black points) used for evaluations of dry deposition. We have moved Fig.6 into SI as suggested (now Fig. S2).

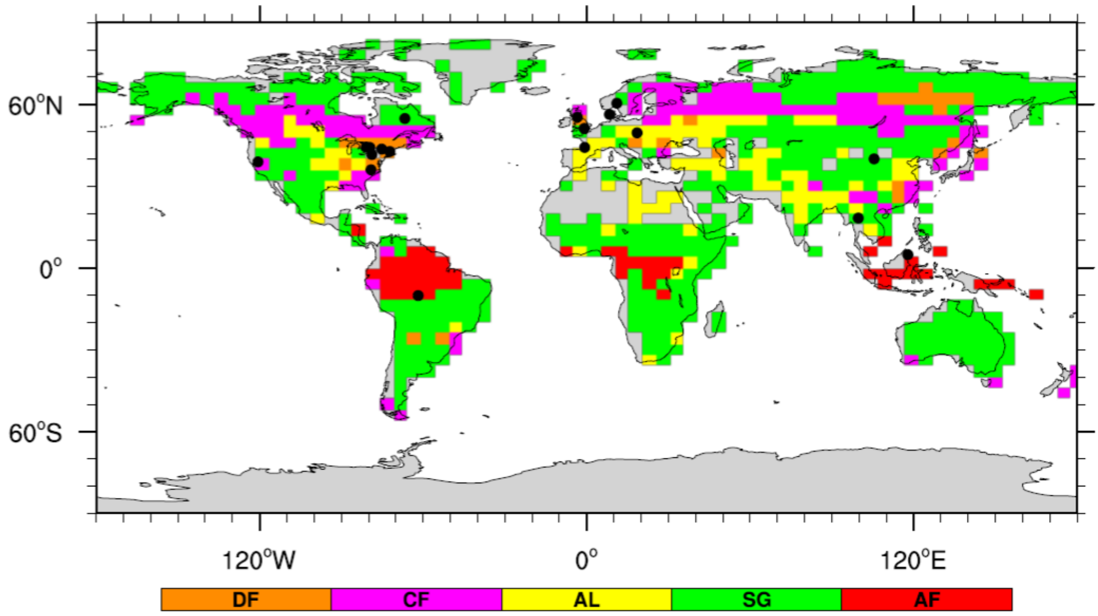

Figure S2 The major dry deposition land type at each grid cell converted from YIBs land types. DF, CF, AL, SG and AF represent deciduous forest, coniferous forest, agricultural land, shrub/grassland and amazon forest, respectively. Black dots indicate the locations of measurement sites used in evaluation (Table 2).

Figure 7: it is unclear which online GC-YIBs conditions were used to generate this figure. Five different online conditions were described in the methods and it should be clarified for each figure which model results are being included. In general, the authors do a good job making this clear, but Fig 7 stands out as an example where

they did not specify this.

Response: Results of online GC-YIBs shown in Figure 7 (now Figure 6) are from simulation Online_ALL. In the revised paper, we clarified in the figure caption as follows: "Figure 6 Comparisons of annual O_3 dry deposition velocity between online GC-YIBs (Online_ALL simulation) and GC (Offline simulation) models for different land types …"

Technical corrections:

Page 13, L. 284: missing a period at the end of the last sentence

Response: Corrected as suggested.

Page 14, L. 290: "[: : :] model overestimates annual [O_3] in southern China while predicts lower values in western Europe [: : :]". "while predicts" is not the correct grammar.

Response: We revised the sentence as follows: "Although offline GC-YIBs model overestimates annual [O3] in southern China <u>and predicts lower</u> values in western Europe and western U.S." (Lines 346-347)

Page 14, L. 300: "GC-YIBs predicts larger [O_3] of 0.5-2 ppbv". I think the authors mean the GC-YIBs predicts HIGHER [O_3] BY 0.5-2 ppbv.

Response: Corrected as suggested.

Response to the reviewer 2

This study represents a new biosphere-chemistry modeling framework that simulates online, two-way interactions between surface ozone and vegetation, mainly through the linkages between stomatal conductance, leaf area index (LAI) and dry deposition. Global model-observation comparison for simulated gross primary productivity (GPP), LAI, ozone concentrations and dry deposition velocities have been conducted using a large ensemble of datasets. This work is important in laying a foundation for more indepth future studies of biosphere-atmosphere interactions. However, as of the current form the manuscript lacks enough details regarding model implementation, which I believe is important for a GMD paper. I would recommend the publication of this manuscript should the following model details are included, addressed and discussed.

➔ Thank you for your positive evaluations. All the questions and concerns have been carefully answered and the paper has been revised accordingly.

Specific comments:

P6 L129: I think here and elsewhere, the units for all variables should be included in all the equations listed.

Response: Units for all equation variables have been added in the revised paper. For Equation (1), we described it as follows: "… where r_s is the leaf stomatal resistance ($s\ m^{-1}$); m is the empirical slope of the Ball-Berry stomatal conductance equation and is affected by water stress; c_s is the CO_2 concentration at the leaf surface ($\mu mol\ m^{-3}$); RH is the relative humidity of atmosphere; b ($m\ s^{-1}$) represents the minimum leaf stomatal conductance when net leaf photosynthesis (A_{net}, $\mu mol\ m^{-2}\ s^{-1}$) is 0." (Lines 147-151)

P7 L137: Carbon allocation and LAI simulations are a very important part of the modeling framework, but no details have been given. The schemes/algorithms used for simulating carbon allocation and LAI should be described.

Response: In the revised paper, we added following descriptions in section 2.1 "Descriptions of the YIBs model" to clarify (Lines 165-184):

The YIBs model applies the LAI and carbon allocation schemes from the TRIFFID model (Cox, 2001;Clark et al., 2011). On the daily scale, canopy LAI is calculated as follows:

$$LAI = f \times LAI_{max} \tag{3}$$

Where f represents phenological factor controlled by meteorological variables (e.g., temperature, water availability, and photoperiod); LAI_{max} represents the available maximum LAI related to tree height, which is dependent on the vegetation carbon content (C_{veg}). The C_{veg} is calculated as follows:

$$C_{veg} = C_l + C_r + C_w \tag{4}$$

where C_l, C_r and C_w represent leaf, root, and stem carbon contents, respectively. And all carbon components are parameterized as the function of LAI_{max}:

$$\begin{cases} C_l = \alpha \times LAI \\ C_r = \alpha \times LAI_{max} \\ C_r = \beta \times LAI_{max}^{\gamma} \end{cases} \tag{5}$$

where α represents the specific leaf carbon density; β and γ represent allometric parameters. The vegetation carbon content C_{veg} is updated every 10 days:

$$\frac{dC_{veg}}{dt} = (1 - \tau) \times NPP - \varphi \tag{6}$$

where τ and φ represent partitioning parameter and litter fall rate, respectively, and their calculation methods have been documented in Yue and Unger (2015). Net primary productivity (*NPP*) is calculated as the residue of subtracting autotrophic respiration (R_a) from GPP:

$$NPP = GPP - R_a \tag{7}$$

P8 L157: Why is aerodynamic resistance not included in the calculation of ozone fluxes? The ozone simulated by any chemical transport model should be at the lowest model layer, but that should be different enough from the ozone concentration at the canopy top. Please justify. Moreover, shouldn't the ozone flux calculated here for ozone damage be consistent with the dry deposition velocity/flux calculation in GC? The internally inconsistent ways to represent ozone fluxes between GC and YIBs seem to reduce the usefulness of GC-YIBs as a coupling tool.

Response: Thank you for the constructive comments.

(i) The GEOS-Chem model calculates concentrations of air components at 47 vertical layers from 1013.25 to 0.01 hPa. We use [O_3] at the lowest layer to approximate O_3 concentration at the canopy top. We acknowledge the limit of this approximation in the discussion section: "(3) [O_3] at the lowest model level is used as an approximation of canopy [O_3]. The current model does not include a sub-grid parameterization of pollution transport within canopy, leading to biases in estimating O_3 vegetation damage and the consequent feedback. However, development of such parameterization is limited by the availability of simultaneous measurements of microclimate and air pollutants." (Lines 506-510)

(ii) In the original YIBs model, O_3 stomatal flux is calculated as the function of boundary layer resistance, stomatal resistance, and ambient O_3 concentration. In order to fully link GEOS-Chem with YIBs, we have updated the stomatal O_3 flux scheme to include aerodynamic resistance (which is now consistent with GEOS-Chem). At each integration step, GEOS-Chem provides both hourly aerodynamic resistance (r_a) and boundary resistance (r_b) for stomatal O_3 flux scheme in YIBs.

In the revised paper, Eq.9 $F_{O_3} = \frac{[O_3]}{r_b+k\cdot r_s}$ has been updated as $F_{O_3} = \frac{[O_3]}{r_a+r_b+k\cdot r_s}$ to take into effects of both r_a and r_b. We clarify in the revised paper as follows: "In the online GC-YIBs configuration, GC provides the hourly meteorology, <u>aerodynamic resistance, boundary layer resistance</u>, and surface [O_3] to YIBs." (Lines 259-261). Accordingly, the assessment of global O_3 damage to vegetation (section 3.3) has been updated. Compared to the original stomatal O_3 flux scheme within YIBs, the new scheme increases O_3 stomatal flux in Amazon but decreases O_3 stomatal flux in eastern China (Fig.R1c). As a result, O_3 damage on GPP decreases in eastern China but increases in Amazon (Fig.R1f).

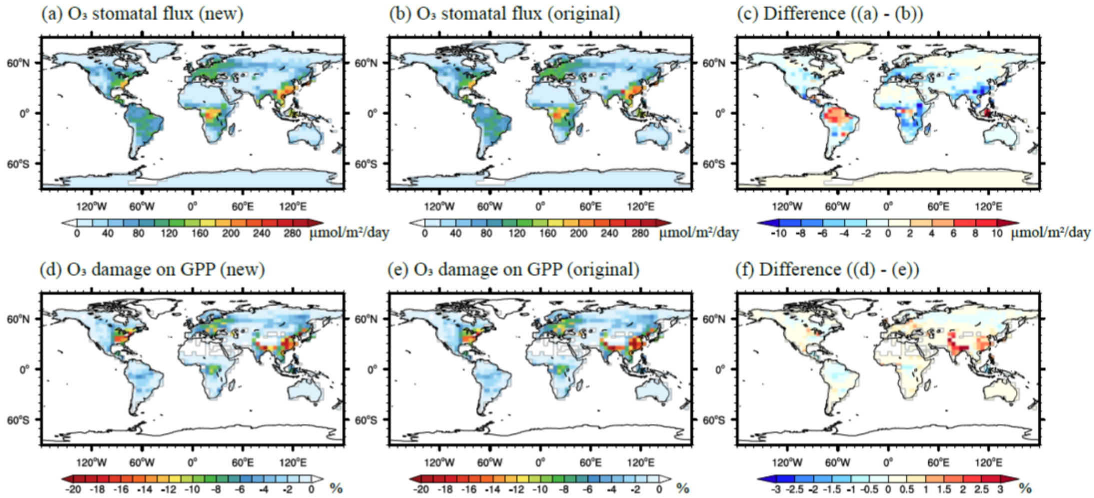

Figure R1 Comparison of O_3 stomatal flux schemes. **(a)** and **(b)** represent the O_3 stomatal flux for new and original schemes, respectively. **(c)** represents the O_3 stomatal flux difference between new and original schemes (a-b). **(d)** and **(e)** represent the O_3 damages to GPP for new and original schemes, respectively. **(f)** represents the O_3 damages difference between new and original schemes (d-e).

P8 L168: 4°×5° appears to be a rather low resolution. While the issue of computational expense is understandable, I recommend the authors to discuss how such a low resolution of simulations may interfere with the accuracy of simulated variables (ozone concentrations, GPP, etc.) as compared with observations.

Response: We run relatively high resolution (2°×2.5°) of GC-YIBs from 2006 to 2007 to have a check. The result of 2007 is used to compare the differences induced by resolutions. The following information has been added in the last part:

"The low resolution will affect local emissions (e.g., NO_x and VOC) and transport, leading to changes in surface [O_3] in GEOS-Chem. The comparison results of 2007 show that low resolution of 4°×5° induces a global mean bias of -0.24 ppbv on surface [O_3] compared to the relatively high resolution at 2°×2.5° (Fig. S7). Compared with surface [O_3], low resolution causes limited differences in vegetation variables (e.g., GPP and LAI, not shown)." (Lines 515-521).

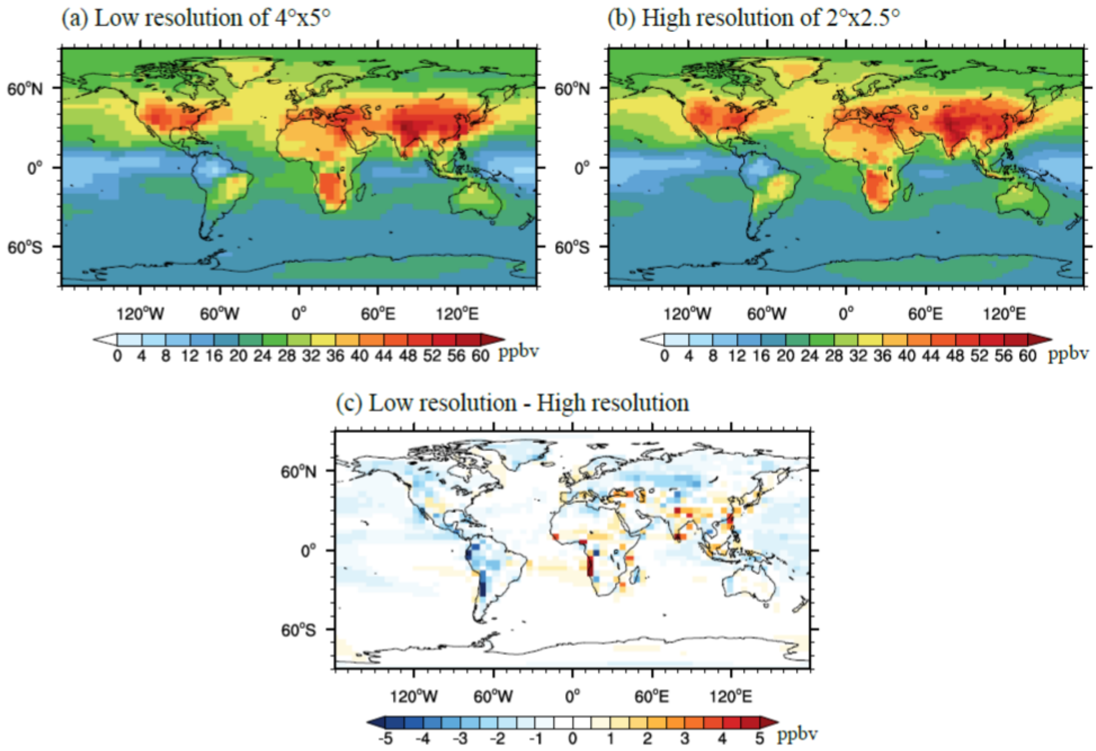

Figure S7 Comparison of MDA8 [O_3] simulated with (a) low (4°×5°) and (b) relatively high (2°×2.5°) horizontal resolutions. (c) represents the MDA8 [O_3] difference between low and high resolutions (a-b).

P10 L210: While the replacement of Olson land-type stomatal resistance with YIBs plant-functional-type (PFT) stomatal resistance is mentioned, could the authors also explain how the conversion of other land-type resistances to YIBs PFT resistances was done? In general, it would be highly useful to explain how Olson land types are matched and mapped with YIBs PFTs. A conversion table in the supplement would really help.

Response: We added Table S2 and Fig. S3 to clarify. In GEOS-Chem, the Olson land-type database are used in the calculation for dry deposition velocity. Each of the Olson land types is assigned a corresponding "deposition land type" with characteristic values of surface resistance components. There are 74 Olson land-types but only 11 deposition land-types (Table R1, i.e., many of the Olson land types share the same deposition characteristics). “The conversion relationships between YIBs land types and GC deposition land types are summarized in Table S2. The global spatial pattern of deposition land types converted from YIBs land types is shown in

Fig. S2. The Olson 2001 land cover map used in GC version 12.0.0 has a native resolution of 0.25°×0.25° and 74 land types (Olson et al., 2001). Each of the Olson land types is associated with a corresponding deposition land type with prescribed parameters. There are 74 Olson land types but only 11 deposition land types, suggesting that many of the Olson land types share the same deposition parameters. At specific grids (4°×5° or 2°×2.5°), dry deposition velocity is calculated as the weighted sum of native resolution (0.25°×0.25°). Replacing of Olson with YIBs land types induces global mean difference of -0.59 ppbv on surface [O_3] (Fig. S3). Large discrepancies are found in Africa and southern Amazon, where the local [O_3] decreases by more than 2 ppbv with the new land types. However, limited differences are shown in mid-high latitudes of Northern Hemisphere (NH, Fig. S3)." (Lines 274-287)

Table R1 The corresponding parameters for 11 deposition land types used in GEOS-Chem (http://wiki.seas.harvard.edu/geos-chem/index.php/Dry_deposition).

DD type	Description	IRI [s m^{-1}]	IRLU [s m^{-1}]	IRAC [s m^{-1}]	IRGSS [s m^{-1}]	IRGSO [s m^{-1}]	IRCLS [s m^{-1}]	IRCLO [s m^{-1}]	IVSMAX [10^{-2} cm s^{-1}]	Reference
1	Snow/Ice	9999	9999	0	100	3500	9999	1000	100	Wesely, AE, 1989
2	Deciduous forest	200	9000	2000	500	200	2000	1000	100	Wesely, AE, 1989
3	Coniferous forest	400	9000	2000	500	200	2000	1000	100	Wesely, AE, 1989
4	Agricultural land	200	9000	200	150	150	2000	1000	100	Wesely, AE, 1989
5	Shrub/grassland	200	9000	100	350	200	2000	1000	100	Wesely, AE, 1989
6	Amazon forest	200	1000	2000	200	200	9999	9999	100	Jacob & Wofsy, JGR 1990
7	Tundra	200	4000	0	340	340	9999	9999	100	Jacob et al., JGR 1992
8	Desert	9999	9999	0	1000	400	9999	9999	10	Wesely, AE, 1989
9	Wetland	200	9000	300	0	1000	2500	1000	100	Wesely, AE, 1989
10	Urban	9999	9999	100	400	300	9999	9999	100	Wesely, AE, 1989
11	Water	9999	9999	0	0	2000	9999	9999	10	Wesely, AE, 1989

Table S2. The conversion relationships between YIBs and GEOS-Chem deposition land types.

YIBs land types	GEOS-Chem deposition land types
Evergreen broadleaf forest	Amazon forest
Evergreen needleleaf forest	Coniferous forest
Deciduous broadleaf forest	Deciduous forest
Shrub land	Shrub/grassland

Tundra	Shrub/grassland
C_4 grasses	Shrub/grassland
C_3 grasses	Shrub/grassland
C_3 crops	Agricultural land
C_4 crops	Agricultural land

P11 L223: YIBs simulates stomatal conductance first at the leaf level, while GC takes in conductance at the canopy level. Appropriate scaling between the two levels should be included and discussed.

Response: In the revised paper, we clarify as follows: "The YIBs model applies Farquhar et al. (1980) scheme to calculate leaf level photosynthesis, which is further upscaled to canopy level by the separation of sunlit and shaded leaves (Spitters, 1986). The canopy is divided into an adaptive number of layers (typically 2-16) for light stratification. Sunlight is attenuated and becomes more diffusive when penetrating the canopy. The sunlit leaves can receive both direct and diffuse radiation, while the shading leaves receive only diffuse radiation. The leaf-level photosynthesis, calculated as the sum of sunlit and shading leaves, is then integrated over all canopy layers to derive the GPP of ecosystems." (Lines 125-133)

P12 L250: Four years of spin-up for LAI simulations is probably insufficient. LAI typically takes decades to stabilize, depending on the initial conditions of LAI. The authors are recommended to explain in greater detail such an issue, show whether LAI has reached a steady state in four years, and state specifically what LAI is used as the initial conditions.

Response: In the GC-YIBs model, the initial soil carbon pool and tree height are provided by the 140-year spin up procedure using offline YIBs. An earlier study (Yue and Unger, 2015) has shown that vegetation variables reached a steady state through 140 years spin up processes. In the "Descriptions of the YIBs model" section, we added: "The initial soil carbon pool and tree height used in YIBs are from the 140 years spin-up processes (Yue and Unger, 2015)". (Lines 138-140)

P14 L306: I think the authors meant Online_GS here instead of Online_LAI.

P15 L308: I think the authors meant Online_LAI here instead of Online_GS.

Response: The simulation names mentioned above are correct. 'Online_LAI' includes online LAI but offline gs, and 'Online_GS' includes online gs but offline LAI. As a result, (Online_ALL – Online_LAI) represents the changes cause by differences in gs (online vs. offline). Meanwhile, (Online_ALL – Online_GS) represents the changes caused by differences in LAI (online vs. offline).

P15 L324: The authors need to justify why BVOC changes resulting from LAI changes are not the dominant factor (in addition to stating the broadly consistent spatial patterns). How BVOC changes should influence the results and interpretation should be discussed in greater detail.

Response: The isoprene and NO_x emissions changes caused by coupled LAI has been added as Fig. S5 in the revised paper. "<u>In a comparison, updated LAI induces limited changes in the isoprene and NO_x emissions (Fig. S5), suggesting that changes of dry deposition velocity are the dominant drivers of O_3 changes</u>". (Lines 379-382) In Fig. 4d, $\Delta[O_3]$ induced by updated LAI show limited changes globally (by 0.05 ppbv) and moderate changes in tropical regions. Such changes mainly because the LAI predicted by YIBs is close to MODIS LAI used in GC (Fig.2).

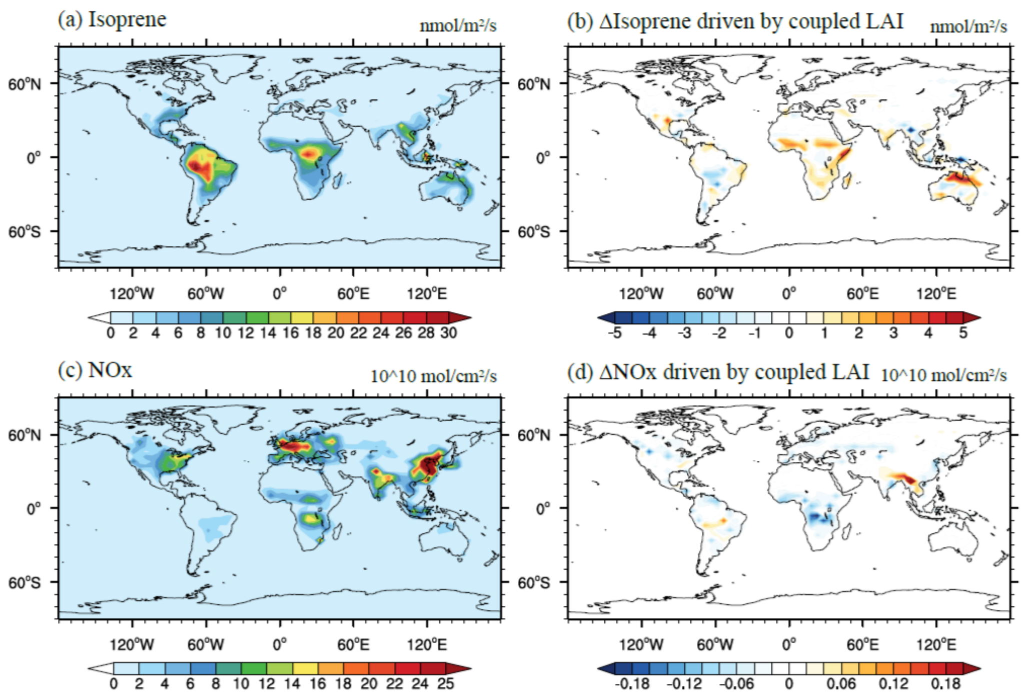

Figure S5 Simulated annual isoprene (a) and NO_x (c) emissions from online GC-YIBs model and its changes (b-d) caused by coupled LAI averaged for period of 2010-2012.

Response to the reviewer 3

This work integrates and couples together a global atmospheric chemistry model (GEOS-Chem) and a terrestrial biosphere model (YIBs) in order to investigate the feedbacks associated between the two, often separately simulated, systems. First, the authors evaluate their integrated model against observed or baseline measures of plant activity (GPP/LAI) and an example chemical species (ozone concentration). They also compare the performance of the coupled and integrated models against observed ozone dry deposition velocities, finding the coupled model an improvement. Using this coupled model, the authors then investigate the impact ozone concentration has on plant activity using differing sensitivities to ozone damage. Overall, this work is timely and addresses an important issue within the modeling of these systems. The description of the model and evaluation is carried-out well with appropriately supportive figures. However, the paper does not go far enough to be truly impactful and confidently useful to the community in its present form, but rather, substantial addition and expansion is required for publishing in GMD. The authors should either expand the evaluation of the model to show that coupling truly does improve comparisons or provide additional applicational evidence for the importance of such coupling to understanding biosphere-atmosphere interactions. Further specific comments and recommendations are listed below.

➔ Thank you for your positive evaluations. All the questions and concerns have been carefully answered and the paper has been revised accordingly.

1) While the PM impact on plants is mentioned as an important process to consider in the introduction (lines 63-69), there is no integration description or evaluation in this paper, and no further mention until the last paragraph. Perhaps clarify the focus of the paper at the beginning to adjust expectations.

Response: We aim to develop a fully coupled biosphere-chemistry model GC-YIBs. We clarify in the introduction section that: “For the first step, we focus on the coupling between O_3 and vegetation. The interactions between aerosols and vegetation will be developed and evaluated in the future." (Lines 113-115) The aerosols-vegetation interaction has been marked with blue dashed box in Fig. 1.

2) Aerosols are not always beneficial to vegetation if the total radiation decreases more than the enhancing effect caused by diffusion (line 64).

Response: The effect of aerosols on vegetation has been modified as following: "Unlike O_3, the effect of aerosols on vegetation is dependent on the aerosol concentrations. Moderate increase of aerosols in the atmosphere is beneficial to vegetation (Schiferl and Heald, 2018;Mahowald, 2011). The aerosol-induced enhancement in diffuse light results in more radiation reaching surface from all directions than solely from above. As a result, leaves in the shade or at the bottom can receive more radiation and are able to assimilate more CO_2 through photosynthesis, leading to an increase of canopy productivity (Mercado et al., 2009;Yue and Unger, 2018). However, excessive aerosol loadings reduce canopy productivity because the total radiation is largely weakened (Yue and Unger, 2017;Alton, 2008)." (Lines 64-73)

3) Since GC-YIBs integrates two existing models, sections 2.1 and 2.2 can be trimmed to only include the relevant equations and processes discussed in the remainder of the paper.

Response: Thank you for your suggestion. Reviewer#2 expects us to add more details about the YIBs model. We have described some important processes within YIBs (e.g., the method calculating LAI, equations 3-7). These descriptions are especially useful to those unfamiliar with the YIBs model.

4) More description of the "satellite-based land types and cover fraction" (lines 122 and 229) would be useful as this is quite vague.

Response: We added Fig. S1 to show the land types used in YIBs. In addition, the conversion relationships between YIBs and GEOS-Chem deposition land types has been added (Table S2 and Fig. S2).

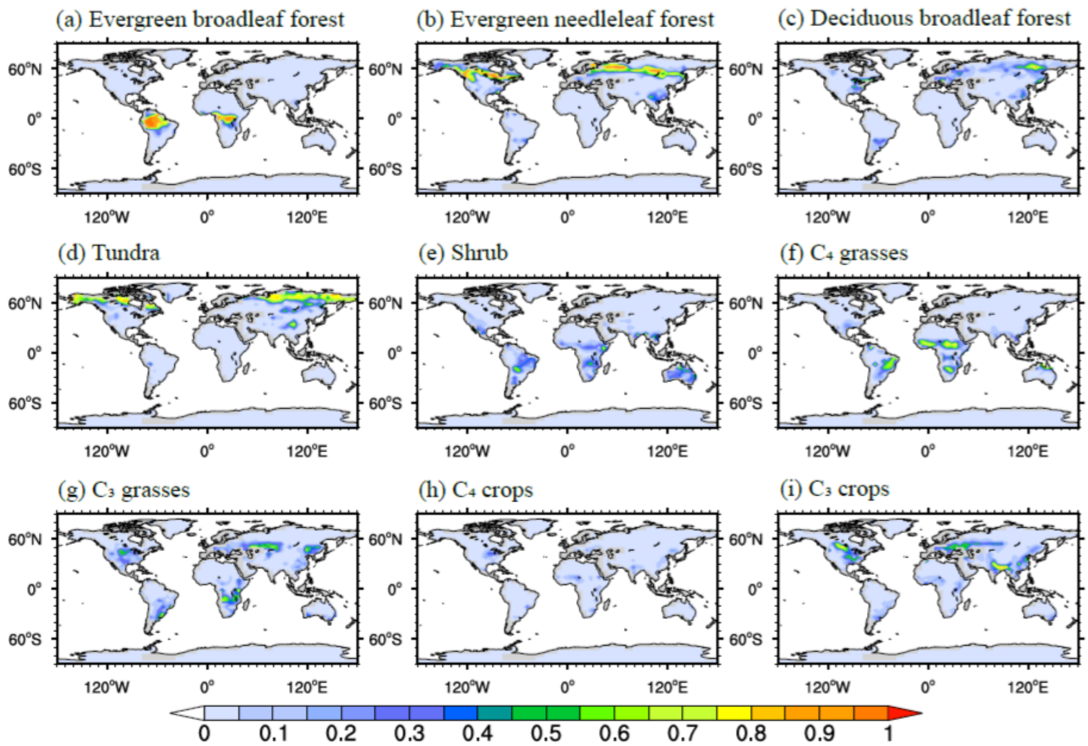

Figure S1 Fractional coverage of each land type at each grid cell.

5) The fact that coefficient α is uncertain and will be varied in different simulations is not clear from the current description in line 153.

Response: We added Table S1 to clarify: "For a specific PFT, the values of coefficient *a* vary from low to high to represent a range of uncertainties for ozone vegetation damaging (Table S1)." (Lines 192-193)

Table S1 The coefficient α of O_3-damaging sensitivity for a specific PFT.

PFTs	α for high sensitivity ($mmol^{-1}\ m^{-2}$)	α for low sensitivity ($mmol^{-1}\ m^{-2}$)
Evergreen broadleaf forest	0.15	0.04
Evergreen needleleaf forest	0.075	0.02
Deciduous broadleaf forest	0.15	0.04

Shrub	0.1	0.03
Tundra	0.1	0.03
C_4 grasses	0.735	0.13
C_3 grasses	1.4	0.25
C_3 crops	1.4	0.25
C_4 crops	0.735	0.13

6) Much work has been done to evaluate the GEOS-Chem dry deposition scheme for ozone and understand the importance of dry deposition schemes in general (e.g. Silva and Heald 2018, JGR, Wong et al 2019, ACP) but these issues are not mentioned here (neither sections 2.2 nor 4). Especially important to consider is lack of observations to truly constrain ozone dry deposition globally and the uncertainty over various timescales and in spatially heterogenous regions.

Response: Related work has been added: "Previous studies have well evaluated the dry deposition scheme used in the GEOS-Chem model against observations globally and regionally (Silva and Heald, 2018;Wong et al., 2019;Hardacre et al., 2015). They found that GEOS-Chem can generally capture the diurnal and seasonal cycles except for the amplitude of O_3 dry deposition velocity (Silva and Heald, 2018)." (Lines 251-255)

7) The title of section 2.5 should read "Evaluation data", as models are evaluated, not validated.

Response: Corrected as suggested.

8) Why are only 9 sites used for the comparison of ozone dry deposition velocity (lines 266, 341-355, Table 2, Figure 8)? Many more data are available as in Silva and Heald 2018.

Response: In revised paper, we expand our evaluations of O_3 dry deposition velocity to 19 sites (27 samples), including Amazon, coniferous and deciduous forests. The data sources are listed in Table 2. The related evaluations have been added and shown in new Figs 7-9 and Fig. S6.

Table 2 List of measurement sites used for dry deposition evaluation.

Land type	Longitude	Latitude	Season	Daytime V_d (cm s^{-1})	References
Deciduous forest	80.9°W	44.3°N	summer	0.92	Padro et al. (1991)
			winter	0.28	
	72.2°W	42.7°N	summer	0.61	Munger et al. (1996)
			winter	0.28	
	75.2°W	43.6°N	summer	0.82	Finkelstein et al. (2000)
	78.8°W	41.6°N	summer	0.83	
	99.7°E	18.3°N	spring	0.38	Matsuda et al. (2005)
			summer	0.65	
	0.84°W	51.17°N	Jul-Aug	0.85	Fowler et al. (2009)
	0.7°W	44.2°N	Jun	0.62	Lamarque et al. (2013)
	79.56°W	44.19°N	summer	0.91	Wu et al. (2016)
Amazon forest	61.8°W	10.1°S	wet	1.1	Rummel et al. (2007)
	117.9°E	4.9°N	wet	1.0	Fowler et al. (2011)
Coniferous forest	3.4°W	55.3°N	spring	0.58	Coe et al. (1995)
	66.7°W	54.8°N	summer	0.26	Munger et al. (1996)
	11.1°E	60.4°N	spring	0.31	Hole et al. (2004)
			summer	0.48	
			autumn	0.2	
			winter	0.074	
	8.4°E	56.3°N	spring	0.68	Mikkelsen et al. (2004)
			summer	0.8	
			autumn	0.83	
	18.53°E	49.55°N	Jul-Aug	0.5	Zapletal et al. (2011)
	79.1°W	36°N	spring	0.79	Finkelstein et al. (2000)
	120.6°W	38.9°N	summer	0.59	Kurpius et al. (2002)
	0.7°W	44.2°N	summer	0.48	Lamaud et al. (1994)
	105.5°E	40°N	summer	0.39	Turnipseed et al. (2009)

9) Given the small sample size and scattered data (Figure 8), the statistics cited for the comparison of dry deposition velocities in coupled GC-YIBs compared to offline GC-YIBs do not provide for high confidence that the model is truly improved with the coupling of these systems (lines 341-355). A more robust analysis should be undertaken to account for the errors in both the observed and simulated values and

present the confidence with which the model could be said to truly be improved.

Response: In the revised paper, we collect data from 19 sites (27 samples) to re-evaluate the model performance in simulating daytime O_3 dry deposition velocity (Fig. 7). Additionally, we evaluate the seasonal and diurnal cycles of simulated O_3 dry deposition velocity (Figs 8 and 9). These updated results show that GC-YIBs indeed improves the performance in simulating daytime O_3 dry deposition velocity and its temporal variability (seasonal and diurnal cycles). The following information has been added in the revised paper:

"We collect long-term measurements from 4 sites across northern America and western Europe to evaluate the model performance in simulating seasonal cycle of O_3 dry deposition velocity (Fig. 8). The GC model well captures the seasonal cycles of O_3 dry deposition velocity in all sites with the correlation coefficients of 0.95 in Harvard, 0.8 in Hyytiala, 0.68 in Ulborg, and 0.71 in Auchencorth. However, the magnitude of O_3 dry deposition velocity is overestimated in Harvard and Hyytiala sites (NME of 60% and 42%, respectively) but underestimated in Ulborg and Auchencorth sites (NME of 48.7% and 58.9%, respectively) at growing seasons. Compared to the GC model, simulated O_3 dry deposition velocity with the GC-YIBs model shows large improvements over Harvard (Hyytiala) sites, where the model-to-observation NME decreases from 60% (42%) to 32% (28%).

Additionally, we investigate the diurnal cycle of O_3 dry deposition velocity at 15 sites (Fig. S6). Observed O_3 dry deposition velocities show single diurnal peak with the maximum from local 8 a.m. to 4 p.m. (Fig. 9). Compared to observations, the GC model has good performance in simulating the diurnal cycle with correlation coefficients of 0.94 for Amazon forest, 0.96 for coniferous forest, and 0.95 for deciduous forest. The GC model underestimates daytime O_3 dry deposition velocity at Amazon forest (NME of 29.8%) but overestimates it at coniferous and deciduous forests (NME of 21.9% and 22.9%, respectively). Compared to the GC model, the simulated daytime O_3 dry deposition velocities using the GC-YIBs model are closer to observations in all three biomes. The NMEs decrease by 9.1% for Amazon forest, 6.8% for coniferous forest, and 7.9% for deciduous forest." (Lines 416-438)

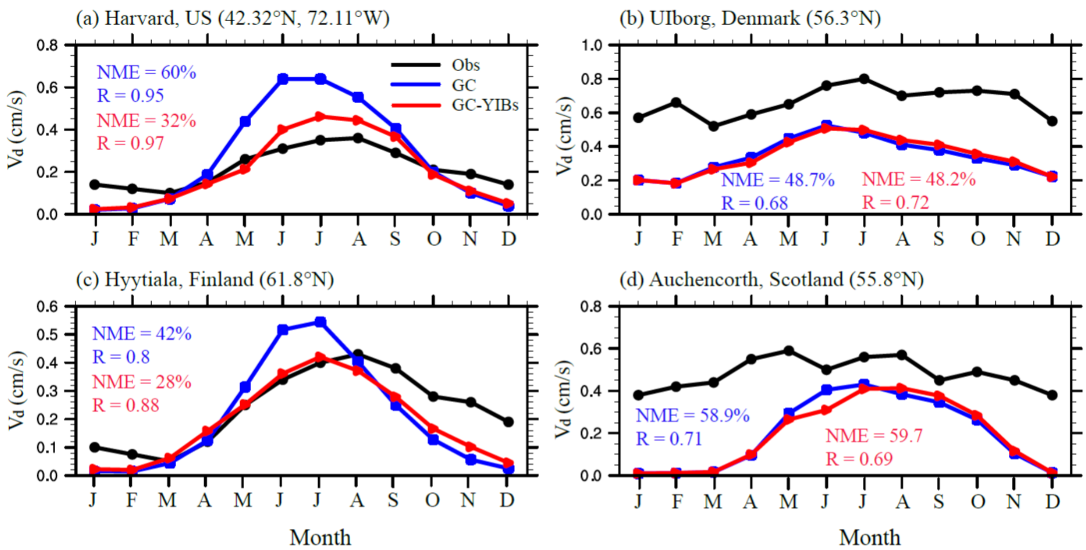

Figure 8 Comparison of monthly O_3 dry deposition velocity at Harvard **(a)**, Ulborg **(b)**, Hyytiala **(c)** and Auchencorth **(d)** sites. The black lines represent observed O_3 dry deposition velocity. The blue and red lines represent simulated O_3 dry deposition velocity from GC (Offline simulation) and GC-YIBs (Online_ALL simulation) models, respectively.

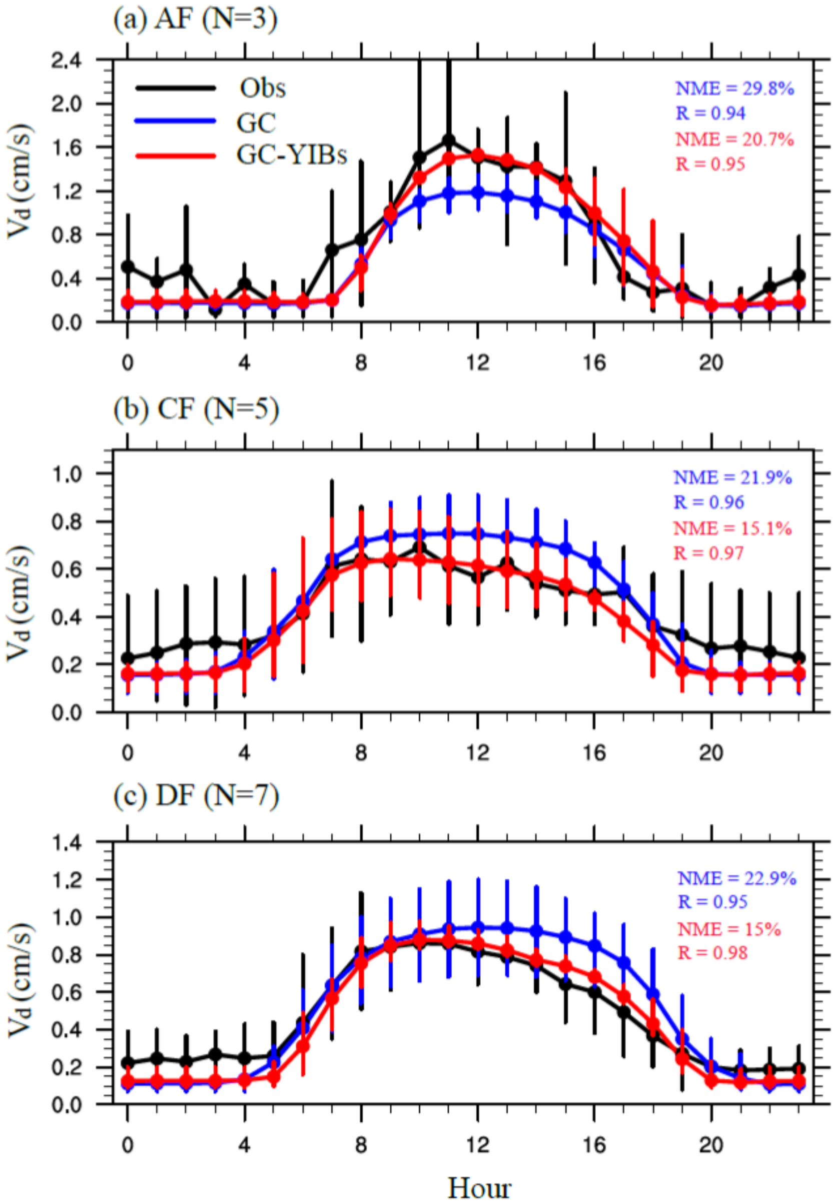

Figure 9 Comparison of multi-site mean diurnal cycle of O_3 dry deposition velocity at Amazon **(a)**, coniferous **(b)** and deciduous **(c)** forests. Error bars represent the range of values from different sites. Black lines represent observed O_3 dry deposition velocity. The blue and red lines represent simulated O_3 dry deposition velocity by GC (Offline simulation) and online GC-YIBs (Online_ALL simulation) models, respectively. The site number (N), R, and NME are shown for each panel.

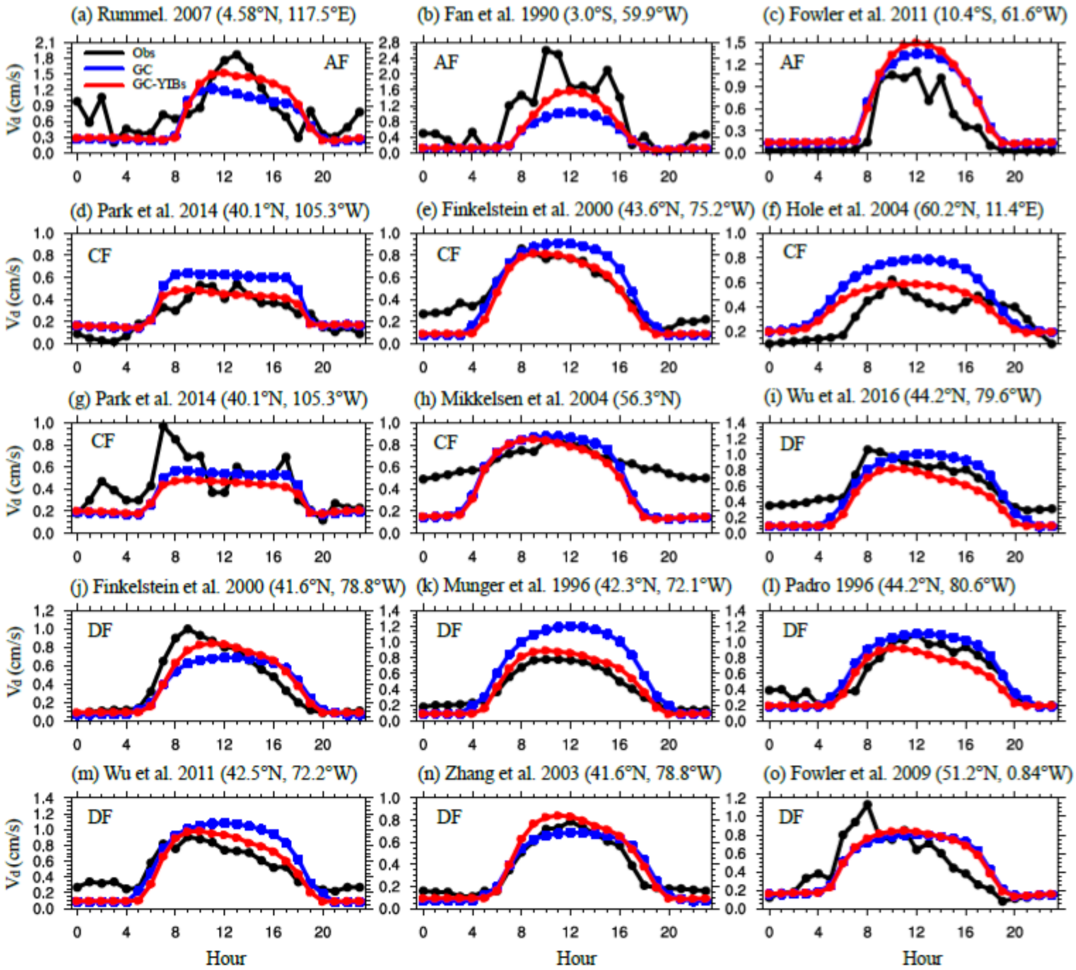

Figure S6 Observed and simulated diurnal cycle of O_3 dry deposition velocity over Amazon (a-c), coniferous (d-h) and deciduous (i-o) forests. The black lines represent observed O_3 dry deposition velocity. The blue and red lines represent simulated O_3 dry deposition velocity from GC (Offline simulation) and GC-YIBs (Online_ALL simulation) models, respectively.

10) Further description of the limitations and errors of both the observed LAI and GPP product should be included (section 2.5), and clarification should be made that GPP is not observed (line 271).

Response: (i) The following information has been added in section 2.5: "Although these products may have certain biases, they have been widely used to evaluate land surface models because direct observations of GPP and LAI are not available on the global scale (Swart et al., 2019;Yue and Unger, 2015;Slevin et al., 2017)." (Lines 315-318) (ii) The original line 271 "The simulated GPP and LAI are compared with observations for the period of 2010-2012 (Fig. 2)." has been revised as "The simulated GPP and LAI are compared with observed LAI and benchmark GPP for the period of 2010-2012 (Fig. 2)."

11) How do the simulated GPP/LAI and ozone concentrations from offline GC-YIBs compare to those values from the original YIBs and GC, respectively? Are the original model configurations degraded or enhanced by the integration and use of a common land type and meteorological driver? Are the magnitudes of these changes similar to the noted improvements seen when the coupling is turned on?

Response: (i) In this study, the simulations in offline YIBs are same as those in the original YIBs. The offline GC is different from original GC. Offline GC calculates O_3 dry deposition velocities using YIBs land types but original GC calculates O_3 dry deposition velocities using Olson land types. The biases induced by different land types has been discussed in section 2.3: "Replacing of Olson with YIBs land types induces global mean difference of -0.59 ppbv on surface [O_3] (Fig. S3). Large discrepancies are found in Africa and southern Amazon, where the local [O_3] decreases by more than 2 ppbv with the new land types. However, limited differences are shown in mid-high latitudes of Northern Hemisphere (NH, Fig. S3)." (Lines 283-287)

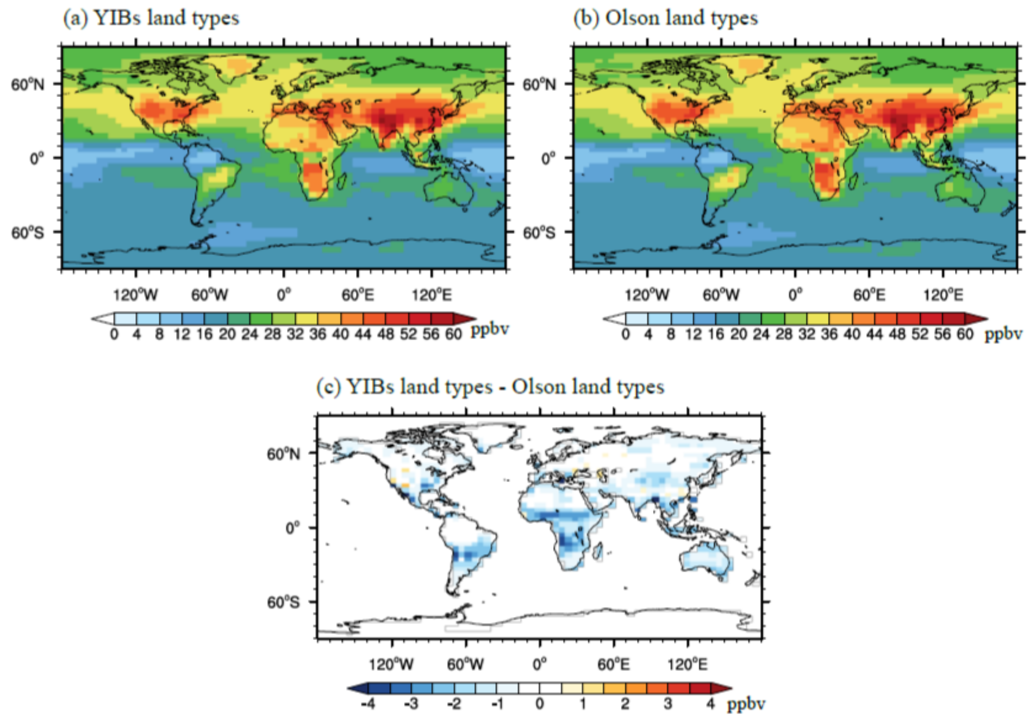

Figure S3 Comparison of YIBs and Olson land types. **(a)** and **(b)** represent the simulated MDA8 [O_3] using YIBs land types and Olson land types, respectively. **(c)** represents the simulated MDA8 [O_3] difference between YIBs and Olson land types.

12) Line 281 attributes the GPP bias to an underestimation in the benchmark GPP for tropical rainforest. Could the differences from using a different meteorology dataset instead be biasing the model (line 283)?

Response: Yue and Unger (2018) showed the YIBs model driven by WFDEI meteorology predicted higher GPP than benchmark in tropical rainforest (Fig. R1). Next, they further evaluated the simulated GPP at evergreen broadleaf forest (EBF) sites from FLUXNET (Fig. R2) and found that YIBs GPP reproduced ground-based observations well. As a result, they concluded that benchmark GPP underestimated the GPP for tropical rainforest. Similar to previous study, our study also reveals a larger GPP predicted by the YIBs model driven by MERRA2 meteorology. We think that such differences between observations and simulations are in part attributed to the underestimation of GPP for tropical rainforest in the benchmark product.

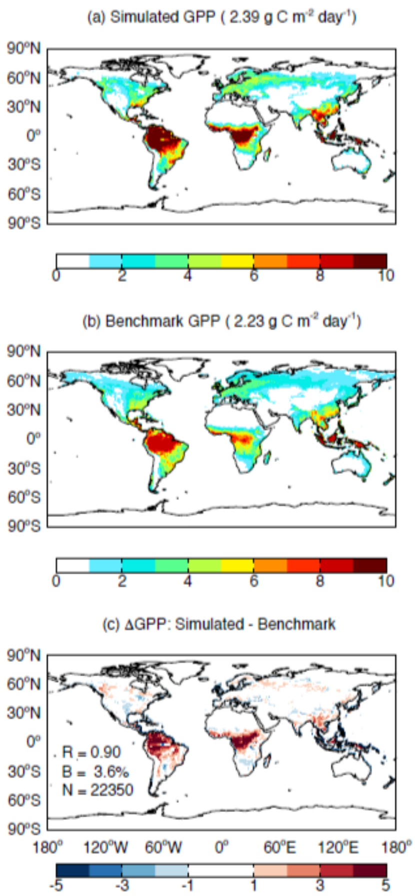

Figure R1 Comparison of YIBs and Benchmark GPP from Yue and Unger (2018).

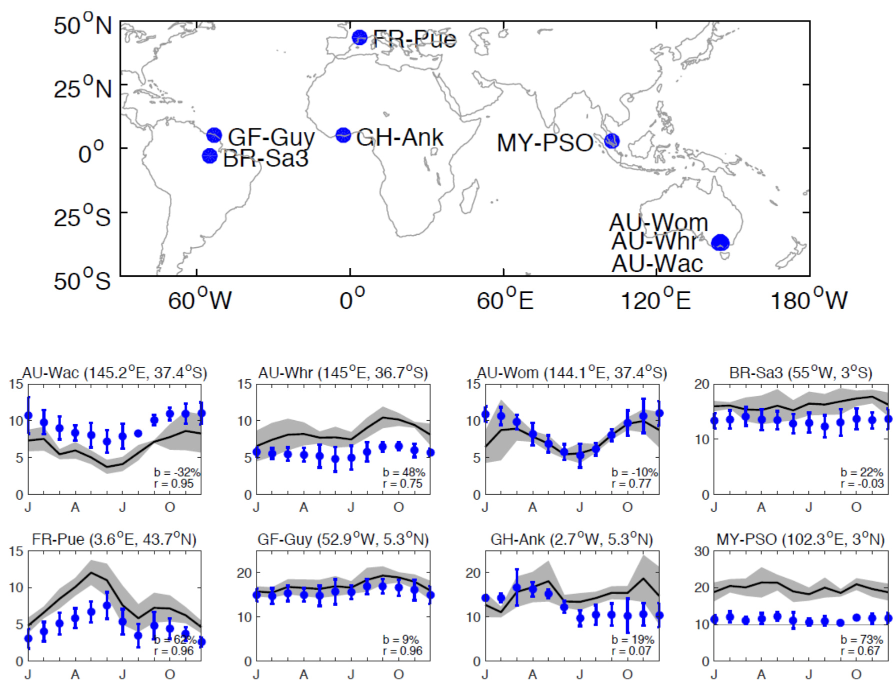

Figure R2 Evaluation of YIBs GPP at EBF sites from Yue and Unger (2018)

13) Compared to what other drivers (BVOC emissions changes?) are dry deposition velocities the dominant driver in the change in O_3 (line 324)? Try testing the impacts of the changing other drivers, rather than relying only on consistent spatial patterns (line 323).

Response: The isoprene and NO_x emission changes caused by coupled LAI has been added as Fig. S5 in the revised paper. The description of this figure has been added "<u>In a comparison, updated LAI induces limited changes in the isoprene and NO_x emissions (Fig. S5), suggesting that changes of dry deposition velocity are the dominant drivers of O_3 changes</u>". (Lines 379-382)

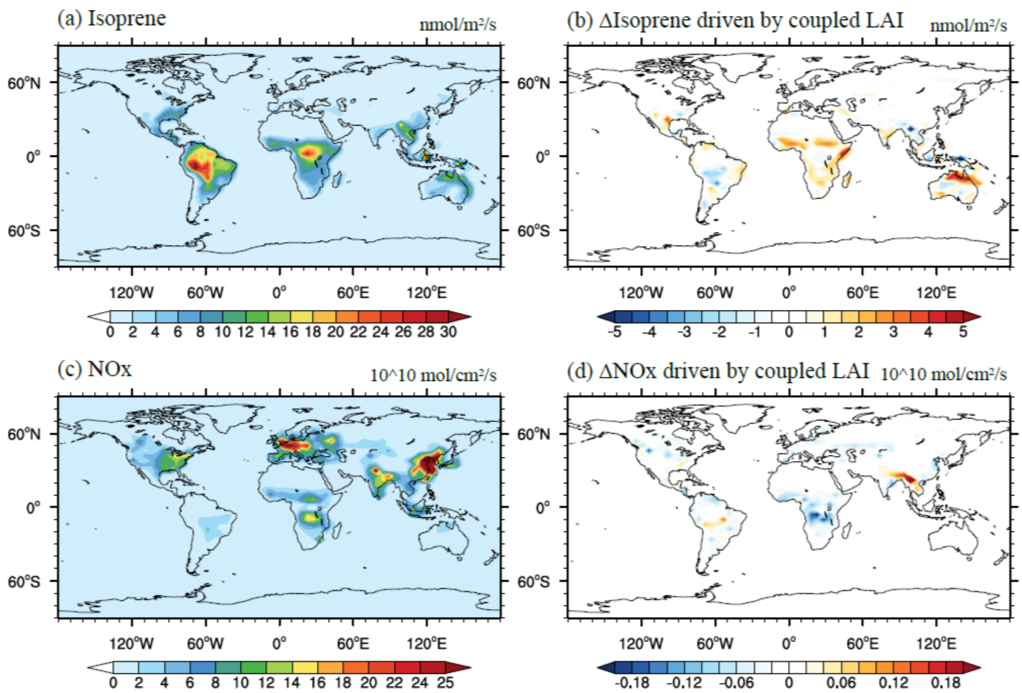

Figure S5 Simulated annual isoprene **(a)** and NO_x **(c)** emissions from online GC-YIBs model and its changes **(b-d)** caused by coupled LAI averaged for period of 2010-2012.

14) The coupling of these systems for the assessment of ozone damages to vegetation is presented as a key motivation for this study, but the differences in damage between this coupled model and previous models are not discussed (mentioned only in line 372). The discussion should be expanded to explain the differences and highlight the advantages of coupling the systems in section 3.3.

Response: The following information has been added in section 3.3:

"The reductions of GPP are slightly higher than our previous estimates using prescribed LAI and/or surface [O_3] in the simulations (Yue and Unger, 2015, 2014), likely because GC-YIBs considers O_3-vegetation interactions. The feedback of such interaction to both chemistry and biosphere will be explored in future studies." (Lines 455-459)

15) Other studies including Lin et al, 2019 GBC for the GFDL models have also investigated the coupled biosphere and atmosphere in similar ways with regards to ozone and are worth discussion in addition to the CESM work. If the ozone dry deposition is the chief application of the model so far, more clarity should be made in the discussion of the uncertainties that already exist in simulating dry deposition globally.

Response: Lin et al. (2019) discussed the influences of different dry deposition schemes on simulated surface [O_3]. They found that using V_d from LM4.0 in an atmospheric chemistry model reduces mean surface [O_3] biases by ~10 ppb relative to the widely used Wesely scheme. However, in their comparisons, they are using different meteorological forcings as the Wesely scheme (in the framework of GEOS-Chem) is driven by MERRA2 reanalyses while the LM4.0 uses another one (http://hydrology.princeton.edu/data.php). As a result, their improvements are jointly contributed by changes in dry deposition and meteorological forcings.

We added following statement to acknowledge the limits and uncertainties of dry deposition schemes: "Although the stomatal conductance scheme of Wesely (1989) has been widely used in chemical transport and climate models, considerable limits still exist because this scheme does not consider the response of stomatal conductance to phenology, CO_2 concentrations, and soil water availability (Rydsaa et al., 2016;Lin et al., 2017). Previous studies have well evaluated the dry deposition scheme used in the GEOS-Chem model against observations globally and regionally (Silva and Heald, 2018;Wong et al., 2019;Hardacre et al., 2015;Lin et al., 2019). They found that GEOS-Chem can generally capture the diurnal and seasonal cycles except for the amplitude of O_3 dry deposition velocity (Silva and Heald, 2018)." (Lines 247-255)

16) One way to justify the slow model speed (line 420) for the modest model improvements shown through coupling would be to expand upon the usefulness of the applications only so far mentioned in lines 428-444.

Response: In the discussion, we first explained the limitations and uncertainties of this study. Then we discussed the importance of this study and the future research plans.

17) While supported in part at Harvard, GEOS-Chem is developed and maintained by a global community of atmospheric chemists, not one group (line 449), and should be acknowledged as such.

Response: Acknowledgement has been modified as "The GEOS-Chem model was developed by the Atmospheric Chemistry Modeling Group at Harvard University led by Prof. Daniel Jacob and <u>improved by a global community of atmospheric chemists</u>." (Line 548)

18) Minor grammatical issues are present throughout, especially omission of articles before nouns. (example, line 48 "from terrestrial biosphere").

Response: Corrected as suggested.

References

Alton, P. B.: Reduced carbon sequestration in terrestrial ecosystems under overcast skies compared to clear skies, Agr Forest Meteorol, 148, 1641-1653, doi:10.1016/j.agrformet.2008.05.014, 2008.

Clark, D., Mercado, L., Sitch, S., Jones, C., Gedney, N., Best, M., Pryor, M., Rooney, G., Essery, R., and Blyth, E.: The Joint UK Land Environment Simulator (JULES), model description–Part 2: carbon fluxes and vegetation dynamics, Geoscientific Model Development, 4, 701-722, 2011.

Coe, H., Gallagher, M. W., Choularton, T. W., and Dore, C.: Canopy scale measurements of stomatal and cuticular O3 uptake by Sitka spruce, Atmospheric Environment, 29, 1413-1423, 1995.

Cox, P. M.: Description of the" TRIFFID" dynamic global vegetation model, 2001.

Farquhar, G. D., Caemmerer, S. V., and Berry, J. A.: A Biochemical-Model of Photosynthetic Co2 Assimilation in Leaves of C-3 Species, Planta, 149, 78-90, doi:Doi 10.1007/Bf00386231, 1980.

Finkelstein, P. L., Ellestad, T. G., Clarke, J. F., Meyers, T. P., Schwede, D. B., Hebert, E. O., and Neal, J. A.: Ozone and sulfur dioxide dry deposition to forests: Observations and model evaluation, J Geophys Res-Atmos, 105, 15365-15377, doi:Doi 10.1029/2000jd900185, 2000.

Fowler, D., Pilegaard, K., Sutton, M. A., Ambus, P., Raivonen, M., Duyzer, J., Simpson, D., Fagerli, H., Fuzzi, S., Schjoerring, J. K., Granier, C., Neftel, A., Isaksen, I. S. A., Laj, P., Maione, M., Monks, P. S., Burkhardt, J., Daemmgen, U., Neirynck, J., Personne, E., Wichink-Kruit, R., Butterbach-Bahl, K., Flechard, C., Tuovinen, J. P., Coyle, M., Gerosa, G., Loubet, B., Altimir, N., Gruenhage, L., Ammann, C., Cieslik, S., Paoletti, E., Mikkelsen, T. N., Ro-Poulsen, H., Cellier, P., Cape, J. N., Horvath, L., Loreto, F., Niinemets, U., Palmer, P. I., Rinne, J., Misztal, P., Nemitz, E., Nilsson, D., Pryor, S., Gallagher, M. W., Vesala, T., Skiba, U., Brueggemann, N., Zechmeister-Boltenstern, S., Williams, J., O'Dowd, C., Facchini, M. C., de Leeuw, G., Flossman, A., Chaumerliac, N., and Erisman, J. W.: Atmospheric composition change: Ecosystems-Atmosphere interactions, Atmospheric Environment, 43, 5193-5267, doi:10.1016/j.atmosenv.2009.07.068, 2009.

Fowler, D., Nemitz, E., Misztal, P., Di Marco, C., Skiba, U., Ryder, J., Helfter, C., Cape, J. N., Owen, S., Dorsey, J., Gallagher, M. W., Coyle, M., Phillips, G., Davison, B., Langford, B., MacKenzie, R., Muller, J., Siong, J., Dari-Salisburgo, C., Di Carlo, P., Aruffo, E., Giammaria, F., Pyle, J. A., and Hewitt, C. N.: Effects of land use on surface-atmosphere exchanges of trace gases and energy in Borneo: comparing fluxes over oil palm plantations and a rainforest, Philos T R Soc B, 366, 3196-3209, doi:10.1098/rstb.2011.0055, 2011.

Hardacre, C., Wild, O., and Emberson, L.: An evaluation of ozone dry deposition in global scale chemistry climate models, Atmospheric Chemistry and Physics, 15, 6419-6436, doi:10.5194/acp-15-6419-2015, 2015.

Hole, L. R., Semb, A., and Torseth, K.: Ozone deposition to a temperate coniferous forest in Norway; gradient method measurements and comparison with the EMEP

deposition module, Atmospheric Environment, 38, 2217-2223, doi:10.1016/j.atmosenv.2003.11.042, 2004.
Kurpius, M. R., McKay, M., and Goldstein, A. H.: Annual ozone deposition to a Sierra Nevada ponderosa pine plantation, Atmospheric Environment, 36, 4503-4515, doi:Pii S1352-2310(02)00423-5
Doi 10.1016/S1352-2310(02)00423-5, 2002.
Lamarque, J. F., Shindell, D. T., Josse, B., Young, P. J., Cionni, I., Eyring, V., Bergmann, D., Cameron-Smith, P., Collins, W. J., Doherty, R., Dalsoren, S., Faluvegi, G., Folberth, G., Ghan, S. J., Horowitz, L. W., Lee, Y. H., MacKenzie, I. A., Nagashima, T., Naik, V., Plummer, D., Righi, M., Rumbold, S. T., Schulz, M., Skeie, R. B., Stevenson, D. S., Strode, S., Sudo, K., Szopa, S., Voulgarakis, A., and Zeng, G.: The Atmospheric Chemistry and Climate Model Intercomparison Project (ACCMIP): overview and description of models, simulations and climate diagnostics, Geoscientific Model Development, 6, 179-206, doi:10.5194/gmd-6-179-2013, 2013.
Lamaud, E., Brunet, Y., Labatut, A., Lopez, A., Fontan, J., and Druilhet, A.: The Landes Experiment - Biosphere-Atmosphere Exchanges of Ozone and Aerosol-Particles above a Pine Forest, J Geophys Res-Atmos, 99, 16511-16521, doi:Doi 10.1029/94jd00668, 1994.
Lin, M. Y., Horowitz, L. W., Payton, R., Fiore, A. M., and Tonnesen, G.: US surface ozone trends and extremes from 1980 to 2014: quantifying the roles of rising Asian emissions, domestic controls, wildfires, and climate, Atmospheric Chemistry and Physics, 17, 2943-2970, doi:10.5194/acp-17-2943-2017, 2017.
Lin, M. Y., Malyshev, S., Shevliakova, E., Paulot, F., Horowitz, L. W., Fares, S., Mikkelsen, T. N., and Zhang, L. M.: Sensitivity of Ozone Dry Deposition to Ecosystem-Atmosphere Interactions: A Critical Appraisal of Observations and Simulations, Global Biogeochem Cy, 33, 1264-1288, doi:10.1029/2018gb006157, 2019.
Mahowald, N.: Aerosol Indirect Effect on Biogeochemical Cycles and Climate, Science, 334, 794-796, doi:10.1126/science.1207374, 2011.
Matsuda, K., Watanabe, I., and Wingpud, V.: Ozone dry deposition above a tropical forest in the dry season in northern Thailand, Atmospheric Environment, 39, 2571-2577, doi:10.1016/j.atmosenv.2005.01.011, 2005.
Mercado, L. M., Bellouin, N., Sitch, S., Boucher, O., Huntingford, C., Wild, M., and Cox, P. M.: Impact of changes in diffuse radiation on the global land carbon sink, Nature, 458, 1014-U1087, doi:10.1038/Nature07949, 2009.
Mikkelsen, T. N., Ro-Poulsen, H., Hovmand, M. F., Jensen, N. O., Pilegaard, K., and Egelov, A. H.: Five-year measurements of ozone fluxes to a Danish Norway spruce canopy, Atmospheric Environment, 38, 2361-2371, doi:10.1016/j.atmosenv.2003.12.036, 2004.
Munger, J. W., Wofsy, S. C., Bakwin, P. S., Fan, S. M., Goulden, M. L., Daube, B. C., Goldstein, A. H., Moore, K. E., and Fitzjarrald, D. R.: Atmospheric deposition of reactive nitrogen oxides and ozone in a temperate deciduous forest and a subarctic woodland .1. Measurements and mechanisms, J Geophys Res-Atmos,

101, 12639-12657, doi:Doi 10.1029/96jd00230, 1996.
Olson, D. M., Dinerstein, E., Wikramanayake, E. D., Burgess, N. D., Powell, G. V. N., Underwood, E. C., D'Amico, J. A., Itoua, I., Strand, H. E., Morrison, J. C., Loucks, C. J., Allnutt, T. F., Ricketts, T. H., Kura, Y., Lamoreux, J. F., Wettengel, W. W., Hedao, P., and Kassem, K. R.: Terrestrial ecoregions of the worlds: A new map of life on Earth, Bioscience, 51, 933-938, doi:Doi 10.1641/0006-3568(2001)051[0933:Teotwa]2.0.Co;2, 2001.
Padro, J., Denhartog, G., and Neumann, H. H.: An Investigation of the Adom Dry Deposition Module Using Summertime O3 Measurements above a Deciduous Forest, Atmos Environ a-Gen, 25, 1689-1704, doi:Doi 10.1016/0960-1686(91)90027-5, 1991.
Rummel, U., Ammann, C., Kirkman, G. A., Moura, M. A. L., Foken, T., Andreae, M. O., and Meixner, F. X.: Seasonal variation of ozone deposition to a tropical rain forest in southwest Amazonia, Atmospheric Chemistry and Physics, 7, 5415-5435, doi:DOI 10.5194/acp-7-5415-2007, 2007.
Rydsaa, J. H., Stordal, F., Gerosa, G., Finco, A., and Hodnebrog, Ø.: Evaluating stomatal ozone fluxes in WRF-Chem: Comparing ozone uptake in Mediterranean ecosystems, Atmospheric environment, 143, 237-248, 2016.
Schiferl, L. D., and Heald, C. L.: Particulate matter air pollution may offset ozone damage to global crop production, Atmospheric Chemistry and Physics, 18, 5953-5966, doi:10.5194/acp-18-5953-2018, 2018.
Silva, S. J., and Heald, C. L.: Investigating Dry Deposition of Ozone to Vegetation, J Geophys Res-Atmos, 123, 559-573, doi:10.1002/2017jd027278, 2018.
Slevin, D., Tett, S. F. B., Exbrayat, J. F., Bloom, A. A., and Williams, M.: Global evaluation of gross primary productivity in the JULES land surface model v3.4.1, Geoscientific Model Development, 10, 2651-2670, doi:10.5194/gmd-10-2651-2017, 2017.
Spitters, C.: Separating the diffuse and direct component of global radiation and its implications for modeling canopy photosynthesis Part II. Calculation of canopy photosynthesis, Agr Forest Meteorol, 38, 231-242, 1986.
Swart, N. C., Cole, J. N. S., Kharin, V. V., Lazare, M., Scinocca, J. F., Gillett, N. P., Anstey, J., Arora, V., Christian, J. R., Hanna, S., Jiao, Y. J., Lee, W. G., Majaess, F., Saenko, O. A., Seiler, C., Seinen, C., Shao, A., Sigmond, M., Solheim, L., von Salzen, K., Yang, D., and Winter, B.: The Canadian Earth System Model version 5 (CanESM5.0.3), Geoscientific Model Development, 12, 4823-4873, doi:10.5194/gmd-12-4823-2019, 2019.
Turnipseed, A. A., Burns, S. P., Moore, D. J. P., Hu, J., Guenther, A. B., and Monson, R. K.: Controls over ozone deposition to a high elevation subalpine forest, Agr Forest Meteorol, 149, 1447-1459, doi:10.1016/j.agrformet.2009.04.001, 2009.
Wong, A. Y. H., Geddes, J. A., Tai, A. P. K., and Silva, S. J.: Importance of dry deposition parameterization choice in global simulations of surface ozone, Atmospheric Chemistry and Physics, 19, 14365-14385, doi:10.5194/acp-19-14365-2019, 2019.
Wu, Z., Staebler, R., Vet, R., and Zhang, L.: Dry deposition of O3 and SO2 estimated

from gradient measurements above a temperate mixed forest, Environmental pollution, 210, 202-210, 2016.
Yue, X., and Unger, N.: Ozone vegetation damage effects on gross primary productivity in the United States, Atmospheric Chemistry and Physics, 14, 9137-9153, doi:10.5194/acp-14-9137-2014, 2014.
Yue, X., and Unger, N.: The Yale Interactive terrestrial Biosphere model version 1.0: description, evaluation and implementation into NASA GISS ModelE2, Geoscientific Model Development, 8, 2399-2417, doi:10.5194/gmd-8-2399-2015, 2015.
Yue, X., and Unger, N.: Aerosol optical depth thresholds as a tool to assess diffuse radiation fertilization of the land carbon uptake in China, Atmospheric Chemistry and Physics, 17, 1329-1342, doi:10.5194/acp-17-1329-2017, 2017.
Yue, X., and Unger, N.: Fire air pollution reduces global terrestrial productivity, Nat Commun, 9, 5413, doi:10.1038/s41467-018-07921-4, 2018.
Zapletal, M., Cudlín, P., Chroust, P., Urban, O., Pokorný, R., Edwards-Jonášová, M., Czerný, R., Janouš, D., Taufarová, K., and Večeřa, Z.: Ozone flux over a Norway spruce forest and correlation with net ecosystem production, Environmental Pollution, 159, 1024-1034, 2011.

Implementation of Yale Interactive terrestrial Biosphere model version 1.0 into GEOS-Chem version 12.0.0: a tool for biosphere-chemistry interactions

Yadong Lei[1,2], Xu Yue[3], Hong Liao[3], Cheng Gong[2,4], Lin Zhang[5]

[1]Climate Change Research Center, Institute of Atmospheric Physics, Chinese Academy of Sciences, Beijing, 100029, China

[2]University of Chinese Academy of Sciences, Beijing, China

[3]Jiangsu Key Laboratory of Atmospheric Environment Monitoring and Pollution Control, Collaborative Innovation Center of Atmospheric Environment and Equipment Technology, School of Environmental Science and Engineering, Nanjing University of Information Science & Technology (NUIST), Nanjing, 210044, China

[4]State Key Laboratory of Atmospheric Boundary Layer Physics and Atmospheric Chemistry (LAPC), Institute of Atmospheric Physics, Chinese Academy of Sciences, Beijing, 100029, China

[5]Laboratory for Climate and Ocean–Atmosphere Studies, Department of Atmospheric and Oceanic Sciences, School of Physics, Peking University, Beijing, 100871, China

Correspondence to: Xu Yue (yuexu@nuist.edu.cn)

Formatted: Font color: Auto

Formatted: Font color: Auto

Formatted: Left, Line spacing: single, Widow/Orphan control

Abstract: The terrestrial biosphere and atmospheric chemistry interact through multiple feedbacks, but the models of vegetation and chemistry are developed separately. In this study, the Yale Interactive terrestrial Biosphere (YIBs) model, a dynamic vegetation model with biogeochemical processes, is implemented into the Chemical Transport Model GEOS-Chem version 12.0.0. Within the GC-YIBs framework, leaf area index (LAI) and canopy stomatal conductance dynamically predicted by YIBs are used for dry deposition calculation in GEOS-Chem. In turn, the simulated surface ozone (O_3) by GEOS-Chem affect plant photosynthesis and biophysics in YIBs. The updated stomatal conductance and LAI improve the simulated O_3 dry deposition velocity and its temporal variability for major tree species. For daytime dry deposition velocities, the model-to-observation correlation increases from 0.69 to 0.76 while the normalized mean error (NME) decreases from 30.5% to 26.9% using the GC-YIBs model. For diurnal cycle, the NMEs decrease by 9.1% for Amazon forest, 6.8% for coniferous forest, and 7.9% for deciduous forest using the GC-YIBs model. Furthermore, we quantify O_3 vegetation damaging effects and find a global reduction of annual gross primary productivity by 1.5-3.6%, with regional extremes of 10.9–14.1% in the eastern U.S. and eastern China. The online GC-YIBs model provides a useful tool for discerning the complex feedbacks between atmospheric chemistry and the terrestrial biosphere under global change.

Keywords: GC-YIBs model, biosphere-chemistry interactions, dry deposition, ozone vegetation damage, evaluations

Deleted: .
Deleted: daytime
Deleted: Compared with the GEOS-Chem model
Deleted: for dry deposition velocities
Formatted: Font color: Auto
Deleted: 76
Deleted: 85
Formatted: Font color: Auto
Formatted: Font color: Auto
Deleted: 35
Deleted: 27%
Formatted: Font color: Auto
Formatted: Font color: Auto
Formatted: Font color: Red
Formatted: Font color: Auto
Formatted: Font color: Auto
Deleted: 2-
Formatted: Font color: Auto
Formatted: Font color: Auto
Deleted: 11–15
Formatted: Font color: Auto
Formatted: Font color: Red
Formatted: Left, Line spacing: single, Widow/Orphan control

1 Introduction

Deleted:

The terrestrial biosphere interacts with atmospheric chemistry through the exchanges of trace gases, water, and energy (Hungate and Koch, 2015; Green et al., 2017). Emissions from the terrestrial biosphere, such as biogenic volatile organic compounds (BVOCs) and nitrogen oxides (NO_x) affect the formation of air pollutants and chemical radicals in the atmosphere (Kleinman, 1994; Li et al., 2019). Globally, the terrestrial biosphere emits ~1100 Tg (1 Tg = 10^{12} g) BVOC annually, which is approximately ten times more than the total amount of VOC emitted worldwide from anthropogenic sources including fossil fuel combustion and industrial activities (Carslaw et al., 2010). Meanwhile, the biosphere acts as a major sink through dry deposition of air pollutants, such as surface ozone (O_3) and aerosols (Petroff, 2005; Fowler et al., 2009; Park et al., 2014). Dry deposition accounts for ~25% of the total O_3 removed from the troposphere (Lelieveld and Dentener, 2000).

Deleted: Green et al., 2017;

Deleted: ; Petroff, 2005

In turn, atmospheric chemistry can also affect the terrestrial biosphere (McGrath et al., 2015; Schiferl and Heald, 2018; Yue and Unger, 2018). Surface O_3 has a negative impact on plant photosynthesis and crop yields by reducing gas-exchange and inducing phytotoxic damages on plant tissues (Van Dingenen et al., 2009; Wilkinson et al., 2012; Yue and Unger, 2014). Unlike O_3, the effect of aerosols on vegetation is dependent on the aerosol concentrations. Moderate increase of aerosols in the atmosphere is beneficial to vegetation (Mahowald, 2011; Schiferl and Heald, 2018). The aerosol-induced enhancement in diffuse light results in more radiation reaching surface from all directions than solely from above. As a result, leaves in the shade or at the bottom

Deleted: Unlike O_3, the

can receive more radiation and are able to assimilate more CO_2 through photosynthesis, leading to an increase of canopy productivity (Mercado et al., 2009; Yue and Unger, 2018). However, excessive aerosol loadings reduce canopy productivity because the total radiation is largely weakened (Alton, 2008; Yue and Unger, 2017).

Models are essential tools to understand and quantify the interactions between the terrestrial biosphere and atmospheric chemistry at the global and/or regional scales. Many studies have performed multiple global simulations with climate-chemistry-biosphere models to quantify the effects of air pollutants on the terrestrial biosphere (Mercado et al., 2009; Yue and Unger, 2015; Oliver et al., 2018; Schiferl and Heald, 2018). In contrast, very few studies have quantified the O_3-induced biogeochemical and meteorological feedbacks to air pollution concentrations (Sadiq et al., 2017; Zhou et al., 2018). Although considerable efforts have been made, uncertainties in biosphere-chemistry interactions remain large because their two-way coupling is not adequately represented in current generation of terrestrial biosphere models or global chemistry models. Global terrestrial biosphere models usually use prescribed O_3 and aerosol concentrations (Sitch et al., 2007; Mercado et al., 2009; Lombardozzi et al., 2012), and global chemistry models often apply fixed offline vegetation variables (Lamarque et al., 2013). For example, stomatal conductance, which plays a crucial role in regulating water cycle and altering pollution deposition, responds dynamically to vegetation biophysics and environmental stressors at various spatiotemporal scales (Hetherington and Woodward, 2003; Franks et al., 2017). However, these processes are either missing

Deleted: ; Yue and Unger, 2015

Deleted: ; Mercado et al., 2009; Sitch et al., 2007

Deleted: Franks et al., 2017;

or lack of temporal variations in most current chemical transport models (Verbeke et al., 2015). The fully two-way coupling between biosphere and chemistry is necessary to better quantify the responses of ecosystems and pollution to global changes.

In this study, we develop the GC-YIBs model by implementing the Yale Interactive terrestrial Biosphere (YIBs) model version 1.0 (Yue and Unger, 2015) into the chemical transport model (CTM) GEOS-Chem version 12.0.0 (http://wiki.seas.harvard.edu/geos-chem/index.php/GEOS-Chem_12#12.0.0). The GEOS-Chem (short as GC thereafter) model has been widely used in episode prediction (Cui et al., 2016), source attribution (D'Andrea et al., 2016; Dunker et al., 2017; Ni et al., 2018; Lu et al., 2019), future pollution projection (Yue et al., 2015; Ramnarine et al., 2019), health risk assessment (Xie et al., 2019), and so on. The standard GC model uses prescribed vegetation parameters and as a result cannot depict the changes in chemical components due to biosphere-pollution interactions. The updated GC-YIBs model links atmospheric chemistry with biosphere in a two-way coupling such that changes in chemical components or vegetation will simultaneously feed back to influence the other systems. Here, we evaluate the dynamically simulated dry deposition and leaf area index (LAI) from GC-YIBs and examine the consequent impacts on surface O_3. We also quantify the detrimental effects of O_3 on gross primary productivity (GPP) using instant pollution concentrations from the chemical module. For the first step, we focus on the coupling between O_3 and vegetation. The interactions between aerosols and vegetation will be developed and evaluated in the future. The next section describes the GC-YIBs

Field Code Changed

Deleted: ; Ni et al., 2018

Deleted: ; Yue et al., 2015

Field Code Changed

model and the evaluation data. Section 3 compares simulated O_3 from GC-YIBs with that from the original GC models and explores the causes of differences. Section 4 quantifies O_3 damaging effects to global GPP using the GC-YIBs model. The last section summarizes progresses and discusses the next-step tasks to optimize the GC-YIBs model.

2 Methods and data

2.1 Descriptions of the YIBs model

YIBs is a terrestrial vegetation model designed to simulate land carbon cycle with dynamical prediction of LAI and tree height (Yue and Unger, 2015). The YIBs model applies Farquhar et al. (1980) scheme to calculate leaf level photosynthesis, which is further upscaled to canopy level by the separation of sunlit and shaded leaves (Spitters, 1986). The canopy is divided into an adaptive number of layers (typically 2-16) for light stratification. Sunlight is attenuated and becomes more diffusive when penetrating the canopy. The sunlit leaves can receive both direct and diffuse radiation, while the shading leaves receive only diffuse radiation. The leaf-level photosynthesis, calculated as the sum of sunlit and shading leaves, is then integrated over all canopy layers to derive the GPP of ecosystems.

The model considers 9 plant functional types (PFTs), including evergreen needleleaf forest, deciduous broadleaf forest, evergreen broadleaf forest, shrubland, tundra, C_3/C_4 grasses, and C_3/C_4 crops. The satellite-based land types and cover fraction are

Deleted: grass

aggregated into these 9 PFTs and used as input (Fig. S1). The initial soil carbon pool and tree height used in YIBs are from the 140 years spin-up processes (Yue and Unger, 2015). The YIBs is driven with hourly 2-D meteorology and 3-D soil variables (6 layers) from the Modern-Era Retrospective analysis for Research and Applications, version 2 (MERRA2).

The YIBs uses the model of Ball and Berry (Baldocchi et al., 1987) to compute leaf stomatal conductance:

$$g_s = \frac{1}{r_s} = m\frac{A_{net}}{c_s}RH + b \tag{1}$$

where r_s is the leaf stomatal resistance $(s\ m^{-1})$; m is the empirical slope of the Ball-Berry stomatal conductance equation and is affected by water stress; c_s is the CO_2 concentration at the leaf surface $(\mu mol\ m^{-3})$; RH is the relative humidity of atmosphere; b $(m\ s^{-1})$ represents the minimum leaf stomatal conductance when net leaf photosynthesis (A_{net}, $\mu mol\ m^{-2}\ s^{-1}$) is 0. For different PFTs, appropriate photosynthetic parameters are derived from the Community Land Model (CLM) (Bonan et al., 2011).

The net leaf photosynthesis for C_3 and C_4 plants is computed based on well-established Michaelis–Menten enzyme-kinetics scheme (Farquhar et al., 1980; Voncaemmerer and Farquhar, 1981):

$$A_{net} = min(J_c, J_e, J_s) - R_d \tag{2}$$

Where J_c, J_e and J_s represent the Rubiso-limited photosynthesis, the RuBP-limited

Deleted: .

Deleted: $g_s = \frac{1}{r_s} = m\frac{A_{net}}{c_s}RH + b$

Deleted: r_s

Deleted: ; m

Deleted: c_s

Deleted: ; RH

Deleted: b

Deleted: carbon assimilation

Deleted: carbon assimilation

Deleted: $A_{net} = \min(J_c, J_e, J_s) - R_d$

Deleted: J_c, J_e

Deleted: J_s

photosynthesis, and the product-limited photosynthesis, respectively. R_d is the rate of dark respiration. They are all parameterized as functions of the maximum carboxylation capacity (Collatz et al., 1991) and meteorological variables (e.g., temperature, radiation, and CO_2 concentrations).

The YIBs model applies the LAI and carbon allocation schemes from the TRIFFID model (Cox, 2001; Clark et al., 2011). On the daily scale, canopy LAI is calculated as follows:

$$LAI = f \times LAI_{max} \quad (3)$$

where f represents phenological factor controlled by meteorological variables (e.g., temperature, water availability, and photoperiod); LAI_{max} represents the available maximum LAI related to tree height, which is dependent on the vegetation carbon content (C_{veg}). The C_{veg} is calculated as follows:

$$C_{veg} = C_l + C_r + C_w \quad (4)$$

where C_l, C_r and C_w represent leaf, root, and stem carbon contents, respectively. And all carbon components are parameterized as the function of LAI_{max}:

$$\begin{cases} C_l = \alpha \times LAI \\ C_r = \alpha \times LAI_{max} \\ C_r = \beta \times LAI_{max}^{\gamma} \end{cases} \quad (5)$$

where α represents the specific leaf carbon density; β and γ represent allometric parameters. The vegetation carbon content C_{veg} is updated every 10 days:

$$\frac{dC_{veg}}{dt} = (1 - \tau) \times NPP - \varphi \quad (6)$$

where τ and φ represent partitioning parameter and litter fall rate, respectively, and their calculation methods have been documented in Yue and Unger (2015). Net primary productivity (NPP) is calculated as the residue of subtracting autotrophic respiration (R_a) from GPP:

$$NPP = GPP - R_a \qquad (7)$$

In addition, the YIBs model implements the scheme for O_3 damage on vegetation proposed by Sitch et al. (2007). The scheme directly modifies photosynthesis using a semi-mechanistic parameterization, which in turn affects stomatal conductance. The O_3 damage factor is considered as the function of stomatal O_3 flux:

$$F = \begin{cases} -a\left(F_{O_3} - T_{O_3}\right), & F_{O_3} > T_{O_3} \\ 0, & F_{O_3} \le T_{O_3} \end{cases} \qquad (8)$$

Where a represents the damaging sensitivity and T_{O_3} represents the O_3 flux threshold ($\mu mol\ m^{-2}\ s^{-1}$). For a specific PFT, the values of coefficient a vary from low to high to represent a range of uncertainties for ozone vegetation damaging (Table S1). T_{O_3} is a critical threshold for O_3 damage and varies with PFTs. The F becomes negative only if F_{O_3} is higher than T_{O_3}. Stomatal O_3 flux F_{O_3} ($\mu mol\ m^{-2}\ s^{-1}$) is calculated as follows:

$$F_{O_3} = \frac{[O_3]}{r_a + r_b + k \cdot r_s} \qquad (9)$$

where $[O_3]$ represents O_3 concentrations at top of the canopy ($\mu mol\ m^{-3}$); r_a is aerodynamic resistance ($s\ m^{-1}$) and r_b is boundary layer resistance ($s\ m^{-1}$); r_s represents stomatal resistance ($s\ m^{-1}$). The Sitch et al. (2007) scheme within the YIBs framework has been well evaluated against hundreds of observations globally (Yue and Unger, 2018) and regionally (Yue et al., 2016; Yue et al., 2017).

Deleted: 3

Deleted: a

Deleted: T_{O_3}

Deleted: .

Formatted: Font:Italic

Deleted: a varies

Deleted: . T_{O_3}

Deleted: F

Deleted: F_{O_3}

Deleted: T_{O_3}.

Deleted: F_{O_3}

Deleted: dependent on both stomatal resistance and ambient $[O_3]$:

Deleted: $F_{O_3} = \frac{[O_3]}{r_b + k \cdot r_s}$ (4

Deleted: $[O_3]$

Deleted: concentration

Deleted: , r_b represents the

Deleted: , and r_s

Deleted: the

Deleted: .

Deleted: Yuan

Deleted: 2017

Deleted: 2016

Deleted:

2.2 Descriptions of the GEOS-Chem model

GC is a global 3-D model of atmospheric compositions with fully coupled O_3-NO_x-hydrocarbon-aerosol chemical mechanisms (Gantt et al., 2015; Lee et al., 2017; Ni et al., 2018). In this study, we use GC version 12.0.0 driven by assimilated meteorology from MERRA2 with a horizontal resolution of 4° latitude by 5° longitude and 47 vertical layers from surface to 0.01 hPa.

In GC, terrestrial vegetation modulates tropospheric O_3 mainly through LAI and canopy stomatal conductance, which affect both the sources and sinks of tropospheric O_3 through changes in BVOC emissions, soil NO_x emissions, and dry deposition (Zhou et al., 2018). BVOC emissions are calculated based on a baseline emission factor parameterized as the function of light, temperature, leaf age, soil moisture, LAI, and CO_2 inhibition within the Model of Emissions of Gasses and Aerosols from Nature (MEGAN v2.1) (Guenther et al., 2006). Soil NO_x emission is computed based on the scheme of Hudman et al. (2012) and further modulated by a reduction factor to account for within-canopy NO_x deposition (Rogers and Whitman, 1991). The dry deposition velocity (V_d, $m\ s^{-1}$) for O_3 is computed based on a resistance-in-series model within GC:

$$V_d = \frac{1}{R_a + R_b + R_c} \qquad (10)$$

where R_a ($m\ s^{-1}$) is the aerodynamic resistance representing the ability of the airflow to bring gases or particles close to the surface and is dependent mainly on the atmospheric turbulence structure and the height considered. R_b ($m\ s^{-1}$) is the

Deleted: (V_d)

Deleted: $V_d = \frac{1}{R_a + R_b + R_c}$ (5

Deleted: R_a

Deleted: R_b

boundary resistance driven by the characteristics of surface (surface roughness) and gas/particle (molecular diffusivity). R_a and R_b are calculated from the global climate models (GCM) meteorological variables (Jacob et al., 1992). The surface resistance R_c is determined by the affinity of surface for the chemical compound. For O_3 over vegetated regions, V_d is mainly driven by R_c ($m\ s^{-1}$) during daytime because the effects of R_a and R_b are generally small. Surface resistances R_c are computed using the Wesely (1989) canopy model with some improvements, including explicit dependence of canopy stomatal resistances on LAI (Gao and Wesely, 1995) and direct/diffuse PAR within the canopy (Baldocchi et al., 1987):

$$\frac{1}{R_c} = \frac{1}{R_s+R_m} + \frac{1}{R_{lu}} + \frac{1}{R_{cl}} + \frac{1}{R_g} \quad (11)$$

where R_s is the stomatal resistance ($s\ m^{-1}$), R_m is the leaf mesophyll resistance (R_m= 0 $s\ m^{-1}$ for O_3), R_{lu} is the upper canopy or leaf cuticle resistance, R_{cl} is the lower canopy resistance ($s\ m^{-1}$). R_s is calculated based on minimum stomatal resistance (r_s, $s\ m^{-1}$), solar radiation (G, $W\ m^{-2}$), surface air temperature (T_s, °C), and the molecular diffusivities (D_{H_2O} and D_x) for a specific gas x:

$$R_s = r_s \left\{1 + \frac{1}{[200(G+0.1)]^2}\right\} \left\{\frac{400}{T_s(40-T_s)}\right\} \frac{D_{H_2O}}{D_x} \quad (12)$$

In GC, the above parameters related to R_c have prescribed values for 11 deposition land types, including snow/ice, deciduous forest, coniferous forest, agricultural land, shrub/grassland, amazon forest, tundra, desert, wetland, urban and water (Wesely, 1989; Jacob et al., 1992).

Although the stomatal conductance scheme of Wesely (1989) has been widely used in

Deleted: R_a and R_b

Deleted: R_c

Deleted: V_d

Deleted: R_c

Deleted: R_a

Deleted: R_b

Deleted: R_c

Deleted: $\frac{1}{R_c} = \frac{1}{R_s+R_m} + \frac{1}{R_{lu}} + \frac{1}{R_{cl}} + \frac{1}{R_g}$ (6

Deleted: R_s

Deleted: , R_m

Deleted: (R_m =

Deleted: s cm^{-1}

Deleted: R_{lu}

Deleted: R_{cl}

Deleted: .

Deleted:),

Deleted:),

Formatted: Font color: Auto

Deleted: ... [1]

Deleted: R_c

Deleted: ; Wesely, 1989

Moved down [1]: The Olson 2001 land cover map used ... [2]

chemical transport and climate models, considerable limits still exist because this scheme does not consider the response of stomatal conductance to phenology, CO_2 concentrations, and soil water availability (Rydsaa et al., 2016; Lin et al., 2017). Previous studies have well evaluated the dry deposition scheme used in the GEOS-Chem model against observations globally and regionally (Hardacre et al., 2015; Silva and Heald, 2018; Lin et al., 2019; Wong et al., 2019). They found that GEOS-Chem can generally capture the diurnal and seasonal cycles except for the amplitude of O_3 dry deposition velocity (Silva and Heald, 2018).

2.3 Implementation of YIBs into GEOS-Chem (GC-YIBs)

In this study, GC model time steps are set to 30 min for transport and convection and 60 min for emissions and chemistry. In the online GC-YIBs configuration, GC provides the hourly meteorology, aerodynamic resistance, boundary layer resistance, and surface $[O_3]$ to YIBs. Without YIBs implementation, the GC model computes O_3 dry deposition velocity using prescribed LAI and parameterized canopy stomatal resistance (R_s), and as a result ignore feedbacks from ecosystems (details in 2.2). With YIBs embedded, daily LAI and hourly stomatal conductance are dynamically predicted for the dry deposition scheme within the GC model. The online-simulated surface $[O_3]$ affects carbon assimilation and canopy stomatal conductance, in turn, the online-simulated vegetation variables such as LAI and stomatal conductance affect both the sources and sinks of O_3 by altering precursor emissions and dry deposition at the 1-hour integration time step. The above processes are summarized in Fig. 1.

Deleted: R_s

Deleted:

To retain the corresponding relationship between vegetation parameters and land cover map in the GC-YIBs model, we replace the Olson 2001 land cover map in GC with satellite-retrieved land cover dataset used by YIBs (Defries et al., 2000; Hanninen and Kramer, 2007). The conversion relationships between YIBs land types and GC deposition land types are summarized in Table S2. The global spatial pattern of deposition land types converted from YIBs land types is shown in Fig. S2. The Olson 2001 land cover map used in GC version 12.0.0 has a native resolution of 0.25°×0.25° and 74 land types (Olson et al., 2001). Each of the Olson land types is associated with a corresponding deposition land type with prescribed parameters. There are 74 Olson land types but only 11 deposition land types, suggesting that many of the Olson land types share the same deposition parameters. At specific grids (4°×5° or 2°×2.5°), dry deposition velocity is calculated as the weighted sum of native resolution (0.25°×0.25°). Replacing of Olson with YIBs land types induces global mean difference of -0.59 ppbv on surface [O_3] (Fig. S3). Large discrepancies are found in Africa and southern Amazon, where the local [O_3] decreases by more than 2 ppbv with the new land types. However, limited differences are shown in mid-high latitudes of Northern Hemisphere (NH, Fig. S3).

2.4 Model simulations

We conduct six simulations to evaluate the performance of GC-YIBs and to quantify global O_3 damage to vegetation (Table 1): (i) Offline, a control run using the offline

Deleted: preserve

Deleted: Stomatal resistance is first calculated for each of 9 PFTs at individual grid cells. The dry deposition velocity is then computed based on the area-weighted sum of stomatal resistance over all PFTs within the same grid.

Moved (insertion) [1]

GC-YIBs model. The YIBs module shares the same meteorological forcing as the GC module and predicts both GPP and LAI. However, predicted vegetation variables are not fed into GC, which is instead driven by prescribed LAI from Moderate Resolution Imaging Spectroradiometer (MODIS) product and parameterized canopy stomatal conductance proposed by Gao and Wesely (1995). (ii) Online_LAI, a sensitive run using online GC-YIBs with dynamically predicted daily LAI from YIBs but prescribed stomatal conductance. (iii) Online_GS, another sensitive run using YIBs predicted stomatal conductance but prescribed MODIS LAI. (iv) Online_ALL, in which both YIBs predicted LAI and stomatal conductance are used for GC. (v) Online_ALL_HS, the same as Online_ALL except that predicted surface O_3 damages plant photosynthesis with high sensitivities. (vi) Online_ALL_LS, the same as Online_ALL_HS but with low O_3 damaging sensitivities. Each simulation is run from 2006 to 2012 with the first 4 years for spin-up, and results from 2010 to 2012 are used to evaluate the online GC-YIBs model. The differences between Online_ALL and Online_GS (Online_LAI) represent the effects of coupled LAI (stomatal conductance) on simulated [O_3]. Differences between Offline and Online_ALL then represent joint effects of coupled LAI and stomatal conductance. The last three runs are used to quantify the global O_3 damage on ecosystem productivity.

Deleted: original parameterizations of

2.5 Evaluation data

Deleted: Validation

We use observed LAI data for 2010–2012 from the MODIS product. Benchmark GPP product of 2010–2012 is estimated by upscaling ground-based FLUXNET eddy covariance data using a model tree ensemble approach, a type of machine learning technique (Jung et al., 2009). Although these products may have certain biases, they have been widely used to evaluate land surface models because direct observations of GPP and LAI are not available on the global scale (Yue and Unger, 2015; Slevin et al., 2017; Swart et al., 2019). Measurements of surface [O_3] over North America and Europe are provided by the Global Gridded Surface Ozone Dataset (Sofen et al., 2016), and those over China are interpolated from data at ~1500 sites operated by China's Ministry of Ecology and Environment (http://english.mee.gov.cn). We perform literature research to collect data of dry deposition velocity from 8 deciduous forest, 2 amazon forest, and 9 coniferous forest sites (Table 2).

3 Results

3.1 Evaluation of offline GC-YIBs model

With Offline simulation, the simulated GPP and LAI are compared with observed LAI and benchmark GPP for the period of 2010-2012 (Fig. 2). Observed LAI and benchmark GPP both show high values in the tropics and medium values in the northern mid-high latitudes. Compared to observations, the GC-YIBs model forced with MERRA2 meteorology depicts similar spatial distributions, with spatial correlation coefficients of 0.83 (p <0.01) for GPP and 0.86 (p <0.01) for LAI. Although the model overestimates LAI in the tropics and northern high latitudes by 1-2 m^2 m^{-2}, the simulated global area-weighted LAI (1.42 m^2 m^{-2}) is close to observations (1.33 m^2 m^{-2}) with a normalized mean bias (NMB) of 6.7%. Similar to LAI, the global NMB for

Deleted: 3

Formatted: Font color: Auto

Deleted: 4

Formatted: Font color: Auto

Deleted: The

Deleted: observations

Formatted: Font color: Auto

Formatted: Font color: Auto

Formatted: Font color: Auto

Formatted: Font color: Auto

Formatted: Font color: Auto

GPP is only 7.1%, though there are substantial regional biases especially in Amazon and central Africa. Such differences are in part attributed to the underestimation of GPP for tropical rainforest in the benchmark product, because the recent simulations at eight rainforest sites with YIBs model reproduced ground-based observations well (Yue and Unger, 2018).

We then evaluate simulated annual mean surface $[O_3]$ during 2010-2012 based on Offline simulation (Fig. 3). The simulated high values are mainly located in the mid-latitudes of NH (Fig. 3a). Compared to observations, simulations show reasonable spatial distribution with a correlation coefficient of 0.63 (p <0.01). Although offline GC-YIBs model overestimates annual $[O_3]$ in southern China and predicts lower values in western Europe and western U.S., the simulated area-weighted surface $[O_3]$ (45.4 ppbv) is only 6% higher than observations (42.8 ppbv). Predicted summertime surface $[O_3]$ instead shows positive biases in eastern U.S. and Europe (Fig. S4), consistent with previous evaluations using the GC model (Travis et al., 2016; Schiferl and Heald, 2018; Yue and Unger, 2018).

3.2 Changes of surface O_3 in online GC-YIBs model

Surface O_3 is changed by the coupling of LAI and stomatal conductance (Fig. 4). Global $[O_3]$ shows similar patterns between Offline (Fig. 3a) and Online_ALL (Fig. 4a) simulations. However, the online GC-YIBs predicts higher $[O_3]$ by 0.5-2 ppbv in the mid-high latitudes of NH, leading to an average enhancement of $[O_3]$ by 0.22 ppbv

Deleted: the YIBs model driven by a different meteorology dataset (Yue and Unger, 2015)

Formatted: Font color: Auto

Formatted: Font color: Auto

Formatted: Font color: Auto

Formatted: Font color: Auto

Deleted: Northern Hemisphere (

Deleted: ,

Formatted: Font color: Auto

Deleted: while

Formatted: Font color: Auto

Deleted: S1

Formatted: Font color: Auto

Formatted: Font color: Auto

Deleted: ; Travis et al., 2016

Formatted: Font color: Auto

Deleted: offline

Deleted: online

Deleted: larger

Deleted: of

compared to Offline simulations (Fig. 4b). Regionally, some negative changes of 1-2 ppbv can be found at the tropical regions. With sensitivity experiments Online_LAI and Online_GS (Table. 1), we separate the contributions of LAI and stomatal conductance changes to $\Delta[O_3]$. It is found that $\Delta[O_3]$ between Online_ALL and Online_LAI (Fig. 4c) resembles the total $\Delta[O_3]$ pattern (Fig. 4b), suggesting that changes in stomatal conductance play the dominant role in regulating surface $[O_3]$. As a comparison, $\Delta[O_3]$ values between Online_ALL and Online_GS show limited changes globally (by 0.05 ppbv) and moderate changes in tropical regions (Fig. 4d), mainly because the LAI predicted by YIBs is close to MODIS LAI used in GC (Fig. 2). It is noticed that the average $\Delta[O_3]$ in Fig. 4b is not equal to the sum of Fig. 4c and Fig. 4d, because of the non-linear effects.

We further explore the possible causes of differences in simulated $[O_3]$ between online and offline GC-YIBs models. Fig. 5 shows simulated annual O_3 dry deposition velocity from online GC-YIBs model and its changes in different sensitivity experiments. The global average velocity is 0.25 cm s^{-1} with regional maximum of 0.5-0.7 cm s^{-1} in tropical rainforest (Fig. 5a), especially over Amazon and central Africa where high ecosystem productivity is observed (Fig. 2). With implementation of YIBs into GC, simulated dry deposition velocity increases over tropical regions but decreases in mid-high latitudes of NH (Fig. 5b). Larger dry deposition results in lower $[O_3]$ in the tropics, while smaller dry deposition increases $[O_3]$ in boreal regions. Such spatial patterns are broadly consistent with $\Delta[O_3]$ in online GC-YIBs (Fig. 4b). In a comparison, updated

Deleted: offline

Deleted: 4b

LAI induces limited changes in the isoprene and NO_x emissions (Fig. S5), suggesting that changes of dry deposition velocity are the dominant drivers of O_3 changes. Both the updated LAI and stomatal conductance influence dry deposition. Sensitivity experiments further show that changes in dry deposition are mainly driven by coupled canopy stomatal conductance (Fig. 5c) instead of LAI (Fig. 5d), though the latter contributes to the enhanced dry deposition in the tropics.

The original GC dry deposition scheme applies fixed parameters for stomatal conductance of a specific land type. The updated GC-YIBs model instead calculates stomatal conductance as a function of photosynthesis and environmental forcings (Equation 1). As a result, predicted dry deposition exhibits discrepancies among biomes. With Offline and Online_ALL simulations, we further evaluate the performance of online GC-YIBs in simulating O_3 dry deposition velocity for specific deposition land types (Fig. 6). For agricultural land and shrub/grassland, the simulated O_3 dry deposition velocity for online GC-YIBs model is close to GC model with NMBs of 3%, -2% and correlation coefficients of 0.96, 0.97, respectively. However, the simulated dry deposition velocity in online GC-YIBs is lower than GC by 18% for deciduous forest and 14% coniferous forest, but larger by 17% for Amazon forest. Such changes match the spatial pattern of dry deposition shown in Fig. 5b.

Since the changes of O_3 dry deposition velocity are mainly found in deciduous forest, coniferous forest, and amazon forest, we collect 27 samples across these three biomes

Deleted: (Fig. 6).

Deleted: (Fig. 7

Formatted: Font color: Auto

Formatted: Font color: Auto

Deleted: data at 9 sites

to evaluate the online GC-YIBs model (Table. 2). For the 11 samples at deciduous forest, the normalized mean error (NME) decreases from 29% in GC model to 24% in GC-YIBs with lower relative errors in 8 sites (Fig. 7). Predictions with the GC-YIBs also show large improvements over coniferous forest, where 8 out of 14 samples showing lower (decreases from 27% in GC to 25% in GC-YIBs) errors. For amazon forest, the GC-YIBs model significantly improves the prediction at one site (117.9°E, 4.9°N) where the original error of -0.17 cm s^{-1} is limited to only 0.03 cm s^{-1}. However, the new model does not improve the prediction at the other amazon forest site. Overall, the simulated daytime O_3 dry deposition velocities in online GC-YIBs model are closer to observations than those in GC model with smaller NME (26.9% vs. 30.5%), root-mean-square errors (RMSE, 0.2 vs. 0.23) and higher correlation coefficients (0.76 vs. 0.69). Such improvements consolidate our strategies in updating GC model to the fully coupled GC-YIBs model.

We collect long-term measurements from 4 sites across northern America and western Europe to evaluate the model performance in simulating seasonal cycle of O_3 dry deposition velocity (Fig. 8). The GC model well captures the seasonal cycles of O_3 dry deposition velocity in all sites with the correlation coefficients of 0.95 in Harvard, 0.8 in Hyytiala, 0.68 in Ulborg, and 0.71 in Auchencorth. However, the magnitude of O_3 dry deposition velocity is overestimated in Harvard and Hyytiala sites (NME of 60% and 42%, respectively) but underestimated in Ulborg and Auchencorth sites (NME of 48.7% and 58.9%, respectively) at growing seasons. Compared to the GC model,

Deleted: and Fig. 6
Deleted: 5
Deleted: 50
Deleted: 27
Deleted: all
Deleted: 8
Deleted: 6
Deleted: 9
Deleted: 48
Deleted: 35
Formatted: Font color: Auto
Formatted: Font color: Auto
Deleted: 27
Deleted: 35
Deleted: 19
Deleted: 24
Deleted: 85
Deleted: 76
Formatted: Font color: Auto
Formatted: Line spacing: double

simulated O_3 dry deposition velocity with the GC-YIBs model shows large improvements over Harvard (Hyytiala) sites, where the model-to-observation NME decreases from 60% (42%) to 32% (28%).

Additionally, we investigate the diurnal cycle of O_3 dry deposition velocity at 15 sites (Fig. S6). Observed O_3 dry deposition velocities show single diurnal peak with the maximum from local 8 a.m. to 4 p.m. (Fig. 9). Compared to observations, the GC model has good performance in simulating the diurnal cycle with correlation coefficients of 0.94 for Amazon forest, 0.96 for coniferous forest, and 0.95 for deciduous forest. The GC model underestimates daytime O_3 dry deposition velocity at Amazon forest (NME of 29.8%) but overestimates it at coniferous and deciduous forests (NME of 21.9% and 22.9%, respectively). Compared to the GC model, the simulated daytime O_3 dry deposition velocities using the GC-YIBs model are closer to observations in all three biomes. The NMEs decrease by 9.1% for Amazon forest, 6.8% for coniferous forest, and 7.9% for deciduous forest.

3.3 Assessment of global O_3 damages to vegetation

An important feature of GC-YIBs is the inclusion of online vegetation damages by surface O_3. Here, we quantify the global O_3 damages to GPP and LAI by conducting Online_ALL_HS and Online_ALL_LS simulations (Fig. 10). Due to O_3 damaging, annual GPP declines from -1.5% (low sensitivity) to -3.6% (high sensitivity) on the global scale. Regionally, O_3 decreases GPP as high as 10.9% in the eastern U.S. and up to 14.1% in eastern China at the high sensitivity (Figs. 10a, b). Such strong damages

Deleted: 9
Formatted: Font color: Auto
Deleted: 2
Formatted: Font color: Auto
Deleted: 5
Formatted: Font color: Auto
Deleted: 11
Deleted: 15
Formatted: Font color: Auto
Deleted: 9a

are related to (i) high ambient [O_3] due to anthropogenic emissions and (ii) large stomatal conductance due to active ecosystem productivity in monsoon areas. The O_3 effects are moderate in tropical areas, where stomatal conductance is also high while [O_3] is very low (Fig. 4a) due to limited anthropogenic emissions. Furthermore, O_3-induced GPP reductions are also small in western U.S. and western Asia. Although [O_3] is high over these semi-arid regions (Fig. 4a), the drought stress decreases stomatal conductance and consequently constrains the O_3 uptake. The damages to LAI (Figs. 10c, d) generally follow the pattern of GPP reductions (Figs. 10a, b) but with lower magnitude. The reductions of GPP are slightly higher than our previous estimates using prescribed LAI and/or surface [O_3] in the simulations (Yue and Unger, 2014, 2015), likely because GC-YIBs considers O_3-vegetation interactions. The feedback of such interaction to both chemistry and biosphere will be explored in future studies.

Deleted: 9c

Deleted: 9a

Deleted: These results

Deleted: different from

Deleted: studies which used

Deleted: .

4 Conclusions and discussion

The terrestrial biosphere and atmospheric chemistry interact through a series of feedbacks (Green et al., 2017). Among biosphere-chemistry interactions, dry deposition plays a key role in the exchange of compounds and acts as an important sink for several air pollutants (Verbeke et al., 2015). However, dry deposition is simply parameterized in most of current CTMs (Hardacre et al., 2015). For all chemical species considered in GC model, stomatal resistance R_c is simply calculated as the function of minimum stomatal resistance and meteorological forcings. Such parameterization not only induces biases, but also ignores the feedbacks from biosphere-chemistry interactions.

Deleted: R_c

For example, recent studies revealed that O_3-induced damages to vegetation could reduce stomatal conductance and in turn alter ambient O_3 level (Sadiq et al., 2017; Zhou et al., 2018). In this study, we implement YIBs into the GC model with fully interactive surface O_3 and the terrestrial biosphere. The dynamically predicted LAI and stomatal conductance from YIBs are instantly provided to GC, meanwhile the prognostic O_3 simulated by GC is simultaneously affecting vegetation biophysics in YIBs. With these updates, simulated O_3 dry deposition velocities and its temporal variability (seasonal and diurnal cycles) in GC-YIBs are closer to observations than those in original GC model.

Deleted: daytime

An earlier study updated dry deposition scheme in the Community Earth System Model (CESM) by implementing the leaf and stomatal resistances (Val Martin et al., 2014). Compared to that work, the magnitudes of $\Delta[O_3]$ in our simulations are smaller in northern America, eastern Europe, and southern China. This might be because the original dry deposition scheme in the GC model (see validation in Fig. 7) is better than that in CESM, leaving limited potentials for improvements. In GC, the leaf cuticular resistance (R_{lu}) is dependent on LAI (Gao and Wesely, 1995), while the original calculation of R_{lu} in CESM does not include LAI (Wesely, 1989). In addition, differences in the canopy schemes for stomatal conductance between YIBs and Community Land Model (CLM) may cause different responses in dry deposition, which is changed by -0.12 to 0.16 cm s^{-1} in GC-YIBs but much larger by -0.15 to 0.25 cm s^{-1} in CESM (Val Martin et al., 2014). Moreover, the GC-YIBs is driven with prescribed

Deleted: R_{lu}

Deleted: R_{lu}

Formatted: Font color: Auto

reanalysis while CESM dynamically predicts climatic variables. Perturbations of meteorology in response to terrestrial properties may further magnify the variations in atmospheric components in CESM.

Although we implement YIBs into GC with fully interactive surface O_3 and the terrestrial biosphere, it should be noted that considerable limits still exist and further developments are required for GC-YIBs. (1) Atmospheric nitrogen alters plant growth and further influences both the sources and sinks of surface O_3 through surface–atmosphere exchange processes (Zhao et al., 2017). However, the YIBs model currently utilizes a fixed nitrogen level and does not include an interactive nitrogen cycle, which may induce uncertainties in simulating carbon fluxes. (2) Validity of $\Delta[O_3]$, especially those at high latitudes in NH, cannot be directly evaluated due to a lack of measurements. Although changes of dry deposition show improvements in GC-YIBs, the ultimate effects on surface $[O_3]$ remain unclear within the original GC framework. (3) $[O_3]$ at the lowest model level is used as an approximation of canopy $[O_3]$. The current model does not include a sub-grid parameterization of pollution transport within canopy, leading to biases in estimating O_3 vegetation damage and the consequent feedback. However, development of such parameterization is limited by the availability of simultaneous measurements of microclimate and air pollutants. (4) The current GC-YIBs is limited to a low resolution due to slow computational speed and high computational costs for long-term integrations. The GC model, even at the 2°×2.5° resolution, takes days to simulate 1 model year due to comprehensive parameterizations

Moved (insertion) [2]

Deleted: (2

of physical and chemical processes. Such low speed constrains long-term spin up required by dynamical vegetation models. The low resolution will affect local emissions (e.g., NO_x and VOC) and transport, leading to changes in surface [O_3] in GEOS-Chem. The comparison results of 2007 show that low resolution of 4°×5° induces a global mean bias of -0.24 ppbv on surface [O_3] compared to the relatively high resolution at 2°×2.5° (Fig. S7). Compared with surface [O_3], low resolution causes limited differences in vegetation variables (e.g., GPP and LAI, not shown).

Deleted: (3

Moved up [2]:) Validity of Δ[O_3], especially those at high latitudes in NH, cannot be directly evaluated due to a lack of measurements. Although changes of dry deposition show improvements in GC-YIBs, the ultimate effects on surface [O_3] remain unclear within the original GC framework.

Despite these deficits, the development of GC-YIBs provides a unique tool for studying biosphere-chemistry interactions. In the future, we will extend our applications in: (1) Air pollution impacts on biosphere, including both O_3 and aerosol effects. The GC-YIBs model can predict atmospheric aerosols, which affect both direct and diffuse radiation through the Rapid Radiative Transfer Model for GCMs (RRTMG) in the GC module (Schiferl and Heald, 2018). The diffuse fertilization effects in the YIBs model have been fully evaluated (Yue and Unger, 2018), and as a result we can quantify the impacts of aerosols on terrestrial ecosystems. (2) Multiple schemes for BVOC emissions. The YIBs model incorporates both MEGAN (Guenther et al., 2006) and photosynthesis-dependent (Unger, 2013) isoprene emission schemes (Yue and Unger, 2015). The two schemes within the GC-YIBs framework can be used and compared for simulations of BVOC and consequent air pollution (e.g., O_3, secondary organic aerosols). (3) Biosphere-chemistry feedbacks to air pollution. The effects of air pollution on the biosphere include changes in stomatal conductance, LAI, and BVOC emissions, which in turn modify the sources and sinks of atmospheric components. Only a few studies have quantified these feedbacks for O_3-vegetation interactions (Sadiq et al., 2017; Zhou et al., 2018). We can explore the full biosphere-chemistry coupling for both O_3 and aerosols using the GC-YIBs model in the future.

Code availability

The YIBs model was developed by Xu Yue and Nadine Unger with code sharing at https://github.com/YIBS01/YIBS_site. The GEOS-Chem model was developed by the Atmospheric Chemistry Modeling Group at Harvard University led by Prof. Daniel Jacob and improved by a global community of atmospheric chemists. The source code for the GEOS-Chem model is publicly available at http://acmg.seas.harvard.edu/geos/. The source codes for the GC-YIBs model is archived at https://github.com/leiyd001/GC-YIBs.

Author contributions. Xu Yue conceived the study. Yadong Lei and Xu Yue were responsible for model coupling, simulations, results analysis and paper writing. All co-authors improved and prepared the manuscript.

Competing interests. The authors declare that they have no conflict of interest.

Acknowledgements. This work is supported by the National Key Research and Development Program of China (grant no. SQ2019YFA060013-02) and National

Natural Science Foundation of China (grant no. 41975155).

References

Alton, P. B.: Reduced carbon sequestration in terrestrial ecosystems under overcast skies compared to clear skies, Agr Forest Meteorol, 148, 1641-1653, 2008.

Baldocchi, D. D., Hicks, B. B., and Camara, P.: A Canopy Stomatal-Resistance Model for Gaseous Deposition to Vegetated Surfaces, Atmospheric Environment, 21, 91-101, 1987.

Bonan, G. B., Lawrence, P. J., Oleson, K. W., Levis, S., Jung, M., Reichstein, M., Lawrence, D. M., and Swenson, S. C.: Improving canopy processes in the Community Land Model version 4 (CLM4) using global flux fields empirically inferred from FLUXNET data, J Geophys Res-Biogeo, 116, 2011.

Carslaw, K. S., Boucher, O., Spracklen, D. V., Mann, G. W., Rae, J. G. L., Woodward, S., and Kulmala, M.: A review of natural aerosol interactions and feedbacks within the Earth system, Atmospheric Chemistry and Physics, 10, 1701-1737, 2010.

Clark, D., Mercado, L., Sitch, S., Jones, C., Gedney, N., Best, M., Pryor, M., Rooney, G., Essery, R., and Blyth, E.: The Joint UK Land Environment Simulator (JULES), model description–Part 2: carbon fluxes and vegetation dynamics, Geoscientific Model Development, 4, 701-722, 2011.

Coe, H., Gallagher, M. W., Choularton, T. W., and Dore, C.: Canopy scale measurements of stomatal and cuticular O3 uptake by Sitka spruce, Atmospheric Environment, 29, 1413-1423, 1995.

Collatz, G. J., Ball, J. T., Grivet, C., and Berry, J. A.: Physiological and Environmental-Regulation of Stomatal Conductance, Photosynthesis and Transpiration - a Model That Includes a Laminar Boundary-Layer, Agr Forest Meteorol, 54, 107-136, 1991.

Cox, P. M.: Description of the" TRIFFID" dynamic global vegetation model, 2001. 2001.

Cui, Y. Z., Lin, J. T., Song, C. Q., Liu, M. Y., Yan, Y. Y., Xu, Y., and Huang, B.: Rapid growth in nitrogen dioxide pollution over Western China, 2005-2013, Atmospheric Chemistry and Physics, 16, 6207-6221, 2016.

D'Andrea, S. D., Ng, J. Y., Kodros, J. K., Atwood, S. A., Wheeler, M. J., Macdonald, A. M., Leaitch, W. R., and Pierce, J. R.: Source attribution of aerosol size distributions and model evaluation using Whistler Mountain measurements and GEOS-Chem-TOMAS simulations, Atmospheric Chemistry and Physics, 16, 383-396, 2016.

Defries, R. S., Hansen, M. C., Townshend, J. R. G., Janetos, A. C., and Loveland, T. R.: A new global 1-km dataset of percentage tree cover derived from remote sensing, Glob Change Biol, 6, 247-254, 2000.

Dunker, A. M., Koo, B., and Yarwood, G.: Contributions of foreign, domestic and natural emissions to US ozone estimated using the path-integral method in CAMx nested within GEOS-Chem, Atmospheric Chemistry and Physics, 17, 12553-12571, 2017.

Farquhar, G. D., Caemmerer, S. V., and Berry, J. A.: A Biochemical-Model of Photosynthetic Co2 Assimilation in Leaves of C-3 Species, Planta, 149, 78-90, 1980.

Finkelstein, P. L., Ellestad, T. G., Clarke, J. F., Meyers, T. P., Schwede, D. B., Hebert, E. O., and Neal, J. A.: Ozone and sulfur dioxide dry deposition to forests: Observations and model evaluation, J Geophys Res-Atmos, 105, 15365-15377, 2000.

Fowler, D., Nemitz, E., Misztal, P., Di Marco, C., Skiba, U., Ryder, J., Helfter, C., Cape, J. N., Owen, S., Dorsey, J., Gallagher, M. W., Coyle, M., Phillips, G., Davison, B., Langford, B., MacKenzie, R., Muller, J., Siong, J., Dari-Salisburgo, C., Di Carlo, P., Aruffo, E., Giammaria, F., Pyle, J. A., and Hewitt, C. N.: Effects of land use on surface-atmosphere exchanges of trace gases and energy in

Formatted: Font:10 pt

Formatted: Indent: Left: 0 cm, Hanging: 1.77 ch, First line: -1.77 ch

Formatted: Font:10 pt

Formatted: Indent: Left: 0 cm, Hanging: 1.77 ch, First line: -1.77 ch

Formatted: Font:10 pt

Formatted: Indent: Left: 0 cm, Hanging: 1.77 ch, First line: -1.77 ch

Formatted: Font:10 pt

Formatted: Indent: Left: 0 cm, Hanging: 1.77 ch, First line: -1.77 ch

Borneo: comparing fluxes over oil palm plantations and a rainforest, Philos T R Soc B, 366, 3196-3209, 2011.

Fowler, D., Pilegaard, K., Sutton, M. A., Ambus, P., Raivonen, M., Duyzer, J., Simpson, D., Fagerli, H., Fuzzi, S., Schjoerring, J. K., Granier, C., Neftel, A., Isaksen, I. S. A., Laj, P., Maione, M., Monks, P. S., Burkhardt, J., Daemmgen, U., Neirynck, J., Personne, E., Wichink-Kruit, R., Butterbach-Bahl, K., Flechard, C., Tuovinen, J. P., Coyle, M., Gerosa, G., Loubet, B., Altimir, N., Gruenhage, L., Ammann, C., Cieslik, S., Paoletti, E., Mikkelsen, T. N., Ro-Poulsen, H., Cellier, P., Cape, J. N., Horvath, L., Loreto, F., Niinemets, U., Palmer, P. I., Rinne, J., Misztal, P., Nemitz, E., Nilsson, D., Pryor, S., Gallagher, M. W., Vesala, T., Skiba, U., Brueggemann, N., Zechmeister-Boltenstern, S., Williams, J., O'Dowd, C., Facchini, M. C., de Leeuw, G., Flossman, A., Chaumerliac, N., and Erisman, J. W.: Atmospheric composition change: Ecosystems-Atmosphere interactions, Atmospheric Environment, 43, 5193-5267, 2009.

Franks, P. J., Berry, J. A., Lombardozzi, D. L., and Bonan, G. B.: Stomatal Function across Temporal and Spatial Scales: Deep-Time Trends, Land-Atmosphere Coupling and Global Models, Plant Physiol, 174, 583-602, 2017.

Gantt, B., Johnson, M. S., Crippa, M., Prevot, A. S. H., and Meskhidze, N.: Implementing marine organic aerosols into the GEOS-Chem model, Geoscientific Model Development, 8, 619-629, 2015.

Gao and Wesely: Modeling gaseous dry deposition over regional scales with satellite observation, Atmosphere Environment, 1995. 1995.

Green, J. K., Konings, A. G., Alemohammad, S. H., Berry, J., Entekhabi, D., Kolassa, J., Lee, J. E., and Gentine, P.: Regionally strong feedbacks between the atmosphere and terrestrial biosphere, Nat Geosci, 10, 410-+, 2017.

Guenther, A., Karl, T., Harley, P., Wiedinmyer, C., Palmer, P. I., and Geron, C.: Estimates of global terrestrial isoprene emissions using MEGAN (Model of Emissions of Gases and Aerosols from Nature), Atmospheric Chemistry and Physics, 6, 3181-3210, 2006.

Hanninen, H. and Kramer, K.: A framework for modelling the annual cycle of trees in boreal and temperate regions, Silva Fenn, 41, 167-205, 2007.

Hardacre, C., Wild, O., and Emberson, L.: An evaluation of ozone dry deposition in global scale chemistry climate models, Atmospheric Chemistry and Physics, 15, 6419-6436, 2015.

Hetherington, A. M. and Woodward, F. I.: The role of stomata in sensing and driving environmental change, Nature, 424, 901-908, 2003.

Hole, L. R., Semb, A., and Torseth, K.: Ozone deposition to a temperate coniferous forest in Norway; gradient method measurements and comparison with the EMEP deposition module, Atmospheric Environment, 38, 2217-2223, 2004.

Hungate, B. A. and Koch, G. W.: Global Environmental Change: Biospheric Impacts and Feedbacks, Encyclopedia of Atmospheric Sciences, 2015. 132-140, 2015.

Jacob, D. J., Wofsy, S. C., Bakwin, P. S., Fan, S. M., Harriss, R. C., Talbot, R. W., Bradshaw, J. D., Sandholm, S. T., Singh, H. B., Browell, E. V., Gregory, G. L., Sachse, G. W., Shipham, M. C., Blake, D. R., and Fitzjarrald, D. R.: Summertime Photochemistry of the Troposphere at High Northern Latitudes, J Geophys Res-Atmos, 97, 16421-16431, 1992.

Jung, M., Reichstein, M., and Bondeau, A.: Towards global empirical upscaling of FLUXNET eddy covariance observations: validation of a model tree ensemble approach using a biosphere model, Biogeosciences, 6, 2001-2013, 2009.

Kleinman, L. I.: Low and High Nox Tropospheric Photochemistry, J Geophys Res-Atmos, 99, 16831-16838, 1994.

Kurpius, M. R., McKay, M., and Goldstein, A. H.: Annual ozone deposition to a Sierra Nevada ponderosa pine plantation, Atmospheric Environment, 36, 4503-4515, 2002.

Lamarque, J. F., Shindell, D. T., Josse, B., Young, P. J., Cionni, I., Eyring, V., Bergmann, D., Cameron-Smith, P., Collins, W. J., Doherty, R., Dalsoren, S., Faluvegi, G., Folberth, G., Ghan, S. J., Horowitz, L. W., Lee, Y. H., MacKenzie, I. A., Nagashima, T., Naik, V., Plummer, D., Righi, M., Rumbold, S. T., Schulz, M., Skeie, R. B., Stevenson, D. S., Strode, S., Sudo, K., Szopa, S., Voulgarakis, A., and Zeng, G.: The Atmospheric Chemistry and Climate Model Intercomparison Project (ACCMIP): overview and description of models, simulations and climate diagnostics, Geoscientific Model Development, 6, 179-206, 2013.

Lamaud, E., Brunet, Y., Labatut, A., Lopez, A., Fontan, J., and Druilhet, A.: The Landes Experiment - Biosphere-Atmosphere Exchanges of Ozone and Aerosol-Particles above a Pine Forest, J Geophys Res-Atmos, 99, 16511-16521, 1994.

Lee, H. M., Park, R. J., Henze, D. K., Lee, S., Shim, C., Shin, H. J., Moon, K. J., and Woo, J. H.: PM2.5 source attribution for Seoul in May from 2009 to 2013 using GEOS-Chem and its adjoint model, Environmental Pollution, 221, 377-384, 2017.

Lelieveld, J. and Dentener, F. J.: What controls tropospheric ozone?, Journal of Geophysical Research: Atmospheres, 105, 3531-3551, 2000.

Li, K., Jacob, D. J., Liao, H., Shen, L., Zhang, Q., and Bates, K. H.: Anthropogenic drivers of 2013-2017 trends in summer surface ozone in China, Proc Natl Acad Sci U S A, 116, 422-427, 2019.

Lin, M. Y., Horowitz, L. W., Payton, R., Fiore, A. M., and Tonnesen, G.: US surface ozone trends and extremes from 1980 to 2014: quantifying the roles of rising Asian emissions, domestic controls, wildfires, and climate, Atmospheric Chemistry and Physics, 17, 2943-2970, 2017.

Lin, M. Y., Malyshev, S., Shevliakova, E., Paulot, F., Horowitz, L. W., Fares, S., Mikkelsen, T. N., and Zhang, L. M.: Sensitivity of Ozone Dry Deposition to Ecosystem-Atmosphere Interactions: A Critical Appraisal of Observations and Simulations, Global Biogeochem Cy, 33, 1264-1288, 2019.

Lombardozzi, D., Levis, S., Bonan, G., and Sparks, J. P.: Predicting photosynthesis and transpiration responses to ozone: decoupling modeled photosynthesis and stomatal conductance, Biogeosciences, 9, 3113-3130, 2012.

Lu, X., Zhang, L., Chen, Y. F., Zhou, M., Zheng, B., Li, K., Liu, Y. M., Lin, J. T., Fu, T. M., and Zhang, Q.: Exploring 2016-2017 surface ozone pollution over China: source contributions and meteorological influences, Atmospheric Chemistry and Physics, 19, 8339-8361, 2019.

Mahowald, N.: Aerosol Indirect Effect on Biogeochemical Cycles and Climate, Science, 334, 794-796, 2011.

Matsuda, K., Watanabe, I., and Wingpud, V.: Ozone dry deposition above a tropical forest in the dry season in northern Thailand, Atmospheric Environment, 39, 2571-2577, 2005.

McGrath, J. M., Betzelberger, A. M., Wang, S. W., Shook, E., Zhu, X. G., Long, S. P., and Ainsworth, E. A.: An analysis of ozone damage to historical maize and soybean yields in the United States, P Natl Acad Sci USA, 112, 14390-14395, 2015.

Mercado, L. M., Bellouin, N., Sitch, S., Boucher, O., Huntingford, C., Wild, M., and Cox, P. M.: Impact of changes in diffuse radiation on the global land carbon sink, Nature, 458, 1014-U1087, 2009.

Formatted: Font:10 pt

Formatted: Indent: Left: 0 cm, Hanging: 1.77 ch, First line: -1.77 ch

Deleted: Geosci

Formatted: Font:10 pt

Deleted: Dev

Formatted: Font:10 pt

Formatted: Font:10 pt

Formatted: Indent: Left: 0 cm, Hanging: 1.77 ch, First line: -1.77 ch

Formatted: Font:10 pt

Formatted: Indent: Left: 0 cm, Hanging: 1.77 ch, First line: -1.77 ch

Formatted: Font:10 pt

Formatted: Indent: Left: 0 cm, Hanging: 1.77 ch, First line: -1.77 ch

Mikkelsen, T. N., Ro-Poulsen, H., Hovmand, M. F., Jensen, N. O., Pilegaard, K., and Egelov, A. H.: Five-year measurements of ozone fluxes to a Danish Norway spruce canopy, Atmospheric Environment, 38, 2361-2371, 2004.

Munger, J. W., Wofsy, S. C., Bakwin, P. S., Fan, S. M., Goulden, M. L., Daube, B. C., Goldstein, A. H., Moore, K. E., and Fitzjarrald, D. R.: Atmospheric deposition of reactive nitrogen oxides and ozone in a temperate deciduous forest and a subarctic woodland .1. Measurements and mechanisms, J Geophys Res-Atmos, 101, 12639-12657, 1996.

Ni, R. J., Lin, J. T., Yan, Y. Y., and Lin, W. L.: Foreign and domestic contributions to springtime ozone over China, Atmospheric Chemistry and Physics, 18, 11447-11469, 2018.

Oliver, R. J., Mercado, L. M., Sitch, S., Simpson, D., Medlyn, B. E., Lin, Y.-S., and Folberth, G. A.: Large but decreasing effect of ozone on the European carbon sink, Biogeosciences, 15, 4245-4269, 2018.

Olson, D. M., Dinerstein, E., Wikramanayake, E. D., Burgess, N. D., Powell, G. V. N., Underwood, E. C., D'Amico, J. A., Itoua, I., Strand, H. E., Morrison, J. C., Loucks, C. J., Allnutt, T. F., Ricketts, T. H., Kura, Y., Lamoreux, J. F., Wettengel, W. W., Hedao, P., and Kassem, K. R.: Terrestrial ecoregions of the worlds: A new map of life on Earth, Bioscience, 51, 933-938, 2001.

Padro, J., Denhartog, G., and Neumann, H. H.: An Investigation of the Adom Dry Deposition Module Using Summertime O3 Measurements above a Deciduous Forest, Atmos Environ a-Gen, 25, 1689-1704, 1991.

Park, R. J., Hong, S. K., Kwon, H. A., Kim, S., Guenther, A., Woo, J. H., and Loughner, C. P.: An evaluation of ozone dry deposition simulations in East Asia, Atmospheric Chemistry and Physics, 14, 7929-7940, 2014.

Petroff, A.: Mechanistic study of aerosol dry deposition on vegetated canopies, Radioprotection, 40, S443-S450, 2005.

Ramnarine, E., Kodros, J. K., Hodshire, A. L., Lonsdale, C. R., Alvarado, M. J., and Pierce, J. R.: Effects of near-source coagulation of biomass burning aerosols on global predictions of aerosol size distributions and implications for aerosol radiative effects, Atmospheric Chemistry and Physics, 19, 6561-6577, 2019.

Rogers, J. E. and Whitman, W. B.: Microbial production and consumption of greenhouse gases: methane, nitrogen oxides, and halomethanes, Journal of Environmental Quality, 23, 211-212, 1991.

Rummel, U., Ammann, C., Kirkman, G. A., Moura, M. A. L., Foken, T., Andreae, M. O., and Meixner, F. X.: Seasonal variation of ozone deposition to a tropical rain forest in southwest Amazonia, Atmospheric Chemistry and Physics, 7, 5415-5435, 2007.

Rydsaa, J. H., Stordal, F., Gerosa, G., Finco, A., and Hodnebrog, Ø.: Evaluating stomatal ozone fluxes in WRF-Chem: Comparing ozone uptake in Mediterranean ecosystems, Atmospheric environment, 143, 237-248, 2016.

Sadiq, M., Tai, A. P. K., Lombardozzi, D., and Val Martin, M.: Effects of ozone–vegetation coupling on surface ozone air quality via biogeochemical and meteorological feedbacks, Atmospheric Chemistry and Physics, 17, 3055-3066, 2017.

Schiferl, L. D. and Heald, C. L.: Particulate matter air pollution may offset ozone damage to global crop production, Atmospheric Chemistry and Physics, 18, 5953-5966, 2018.

Silva, S. J. and Heald, C. L.: Investigating Dry Deposition of Ozone to Vegetation, J Geophys Res-Atmos, 123, 559-573, 2018.

Formatted: Font:10 pt

Formatted: Indent: Left: 0 cm, Hanging: 1.77 ch, First line: -1.77 ch

Formatted: Font:10 pt

Formatted: Indent: Left: 0 cm, Hanging: 1.77 ch, First line: -1.77 ch

Sitch, S., Cox, P. M., Collins, W. J., and Huntingford, C.: Indirect radiative forcing of climate change through ozone effects on the land-carbon sink, Nature, 448, 791-794, 2007.

Slevin, D., Tett, S. F. B., Exbrayat, J. F., Bloom, A. A., and Williams, M.: Global evaluation of gross primary productivity in the JULES land surface model v3.4.1, Geoscientific Model Development, 10, 2651-2670, 2017.

Sofen, E. D., Bowdalo, D., Evans, M. J., Apadula, F., Bonasoni, P., Cupeiro, M., Ellul, R., Galbally, I. E., Girgzdiene, R., and Luppo, S.: Gridded global surface ozone metrics for atmospheric chemistry model evaluation, Earth System Science Data,8,1(2016-02-11), 8, 603-647, 2016.

Spitters, C.: Separating the diffuse and direct component of global radiation and its implications for modeling canopy photosynthesis Part II. Calculation of canopy photosynthesis, Agr Forest Meteorol, 38, 231-242, 1986.

Swart, N. C., Cole, J. N. S., Kharin, V. V., Lazare, M., Scinocca, J. F., Gillett, N. P., Anstey, J., Arora, V., Christian, J. R., Hanna, S., Jiao, Y. J., Lee, W. G., Majaess, F., Saenko, O. A., Seiler, C., Seinen, C., Shao, A., Sigmond, M., Solheim, L., von Salzen, K., Yang, D., and Winter, B.: The Canadian Earth System Model version 5 (CanESM5.0.3), Geoscientific Model Development, 12, 4823-4873, 2019.

Travis, K. R., Jacob, D. J., Fisher, J. A., Kim, P. S., Marais, E. A., Zhu, L., Yu, K., Miller, C. C., Yantosca, R. M., Sulprizio, M. P., Thompson, A. M., Wennberg, P. O., Crounse, J. D., St Clair, J. M., Cohen, R. C., Laughner, J. L., Dibb, J. E., Hall, S. R., Ullmann, K., Wolfe, G. M., Pollack, I. B., Peischl, J., Neuman, J. A., and Zhou, X. L.: Why do models overestimate surface ozone in the Southeast United States?, Atmospheric Chemistry and Physics, 16, 13561-13577, 2016.

Turnipseed, A. A., Burns, S. P., Moore, D. J. P., Hu, J., Guenther, A. B., and Monson, R. K.: Controls over ozone deposition to a high elevation subalpine forest, Agr Forest Meteorol, 149, 1447-1459, 2009.

Unger, N.: Isoprene emission variability through the twentieth century, J Geophys Res-Atmos, 118, 13606-13613, 2013.

Val Martin, M., Heald, C. L., and Arnold, S. R.: Coupling dry deposition to vegetation phenology in the Community Earth System Model: Implications for the simulation of surface O3, Geophysical Research Letters, 41, 2988-2996, 2014.

Van Dingenen, R., Dentener, F. J., Raes, F., Krol, M. C., Emberson, L., and Cofala, J.: The global impact of ozone on agricultural crop yields under current and future air quality legislation, Atmospheric Environment, 43, 604-618, 2009.

Verbeke, T., Lathière, J., Szopa, S., and de Noblet-Ducoudré, N.: Impact of future land-cover changes on HNO₃ and O₃ surface dry deposition, Atmospheric Chemistry and Physics, 15, 13555-13568, 2015.

Voncaemmerer, S. and Farquhar, G. D.: Some Relationships between the Biochemistry of Photosynthesis and the Gas-Exchange of Leaves, Planta, 153, 376-387, 1981.

Wesely: Parameterization of surface resistances to gaseous drydeposition in regional-scale numerical models, 1989. 1989.

Wilkinson, S., Mills, G., Illidge, R., and Davies, W. J.: How is ozone pollution reducing our food supply?, J Exp Bot, 63, 527-536, 2012.

Wong, A. Y. H., Geddes, J. A., Tai, A. P. K., and Silva, S. J.: Importance of dry deposition parameterization choice in global simulations of surface ozone, Atmospheric Chemistry and Physics, 19, 14365-14385, 2019.

Formatted: Font:10 pt

Formatted: Indent: Left: 0 cm, Hanging: 1.77 ch, First line: -1.77 ch

Formatted: Font:10 pt

Formatted: Indent: Left: 0 cm, Hanging: 1.77 ch, First line: -1.77 ch

Formatted: Font:10 pt

Formatted: Indent: Left: 0 cm, Hanging: 1.77 ch, First line: -1.77 ch

Formatted: Font:10 pt

Formatted: Indent: Left: 0 cm, Hanging: 1.77 ch, First line: -1.77 ch

Deleted: HNO3 and O3

Formatted: Font:10 pt

Wu, Z., Staebler, R., Vet, R., and Zhang, L.: Dry deposition of O3 and SO2 estimated from gradient measurements above a temperate mixed forest, Environmental pollution, 210, 202-210, 2016.

Xie, Y., Dai, H. C., Zhang, Y. X., Wu, Y. Z., Hanaoka, T., and Masui, T.: Comparison of health and economic impacts of PM2.5 and ozone pollution in China, Environ Int, 130, 2019.

Yue, X., Keenan, T. F., Munger, W., and Unger, N.: Limited effect of ozone reductions on the 20-year photosynthesis trend at Harvard forest, Glob Change Biol, 22, 3750-3759, 2016.

Yue, X., Mickley, L. J., Logan, J. A., Hudman, R. C., Martin, M. V., and Yantosca, R. M.: Impact of 2050 climate change on North American wildfire: consequences for ozone air quality, Atmospheric Chemistry and Physics, 15, 10033-10055, 2015.

Yue, X. and Unger, N.: Aerosol optical depth thresholds as a tool to assess diffuse radiation fertilization of the land carbon uptake in China, Atmospheric Chemistry and Physics, 17, 1329-1342, 2017.

Yue, X. and Unger, N.: Fire air pollution reduces global terrestrial productivity, Nat Commun, 9, 5413, 2018.

Yue, X. and Unger, N.: Ozone vegetation damage effects on gross primary productivity in the United States, Atmospheric Chemistry and Physics, 14, 9137-9153, 2014.

Yue, X. and Unger, N.: The Yale Interactive terrestrial Biosphere model version 1.0: description, evaluation and implementation into NASA GISS ModelE2, Geoscientific Model Development, 8, 2399-2417, 2015.

Yue, X., Unger, N., Harper, K., Xia, X. G., Liao, H., Zhu, T., Xiao, J. F., Feng, Z. Z., and Li, J.: Ozone and haze pollution weakens net primary productivity in China, Atmospheric Chemistry and Physics, 17, 6073-6089, 2017.

Zapletal, M., Cudlín, P., Chroust, P., Urban, O., Pokorný, R., Edwards-Jonášová, M., Czerný, R., Janouš, D., Taufarová, K., and Večeřa, Z.: Ozone flux over a Norway spruce forest and correlation with net ecosystem production, Environmental Pollution, 159, 1024-1034, 2011.

Zhao, Y., Zhang, L., Tai, A. P. K., Chen, Y., and Pan, Y.: Responses of surface ozone air quality to anthropogenic nitrogen deposition in the Northern Hemisphere, Atmospheric Chemistry and Physics, 17, 9781-9796, 2017.

Zhou, S. S., Tai, A. P. K., Sun, S., Sadiq, M., Heald, C. L., and Geddes, J. A.: Coupling between surface ozone and leaf area index in a chemical transport model: strength of feedback and implications for ozone air quality and vegetation health, Atmospheric Chemistry and Physics, 18, 14133-14148, 2018.

Formatted: Font:10 pt

Formatted: Indent: Left: 0 cm, Hanging: 1.77 ch, First line: -1.77 ch

Deleted: Yuan, X. Y., Feng, Z. Z., Liu, S., Shang, B., Li, P., Xu, Y. S., and Paoletti, E.: Concentration-and flux-based dose-responses of isoprene emission from poplar leaves and plants exposed to an ozone concentration gradient, Plant Cell Environ, 40, 1960-1971, 2017.

Formatted: Font:10 pt

Formatted: Indent: Left: 0 cm, Hanging: 1.77 ch, First line: -1.77 ch

Formatted: Font:10 pt

Formatted: Font:10 pt

Formatted: Indent: Left: 0 cm, Hanging: 1.77 ch, First line: -1.77 ch

Formatted: Indent: Left: 0 cm, Hanging: 1.77 ch, First line: -1.77 ch

Table 1 Summary of simulations using the GC-YIBs model.

Name	Scheme	Ozone effects
Offline	Monthly prescribed MODIS LAI	No
	Original dry deposition scheme	
Online_LAI	Daily dynamically predicted LAI	No
	Original dry deposition scheme	
Online_GS	Monthly prescribed MODIS LAI	No
	Hourly predicted stomatal conductance	
Online_ALL	Daily dynamically predicted LAI	No
	Hourly predicted stomatal conductance	
Online_ALL_HS	Daily dynamically predicted LAI	
	Hourly predicted stomatal conductance	High
	Hourly predicted [O_3] by GC model	
Online_ALL_LS	Daily dynamically predicted LAI	
	Hourly predicted stomatal conductance	Low
	Hourly predicted [O_3] by GC model	

Table 2 List of measurement sites used for dry deposition evaluation.

Land type	Longitude	Latitude	Season	Daytime V_d (cm s^{-1})	References
Deciduous forest	80.9°W	44.3°N	summer	0.92	Padro et al. (1991)
			winter	0.28	
	72.2°W	42.7°N	summer	0.61	Munger et al. (1996)
			winter	0.28	
	75.2°W	43.6°N	summer	0.82	Finkelstein et al. (2000)
	78.8°W	41.6°N	summer	0.83	
	99.7°E	18.3°N	spring	0.38	Matsuda et al. (2005)
			summer	0.65	
	0.84°W	51.17°N	Jul-Aug	0.85	Fowler et al. (2009)
	0.7°W	44.2°N	Jun	0.62	Lamarque et al. (2013)
	79.56°W	44.19°N	summer	0.91	Wu et al. (2016)
Amazon forest	61.8°W	10.1°S	wet	1.1	Rummel et al. (2007)
	117.9°E	4.9°N	wet	1.0	Fowler et al. (2011)
Coniferous forest	3.4°W	55.3°N	spring	0.58	Coe et al. (1995)
	66.7°W	54.8°N	summer	0.26	Munger et al. (1996)
	11.1°E	60.4°N	spring	0.31	Hole et al. (2004)
			summer	0.48	
			autumn	0.2	
			winter	0.074	
	8.4°E	56.3°N	spring	0.68	Mikkelsen et al. (2004)
			summer	0.8	
			autumn	0.83	
	18.53°E	49.55°N	Jul-Aug	0.5	Zapletal et al. (2011)
	79.1°W	36°N	spring	0.79	Finkelstein et al. (2000)
	120.6°W	38.9°N	summer	0.59	Kurpius et al. (2002)
	0.7°W	44.2°N	summer	0.48	Lamaud et al. (1994)
	105.5°E	40°N	summer	0.39	Turnipseed et al. (2009)

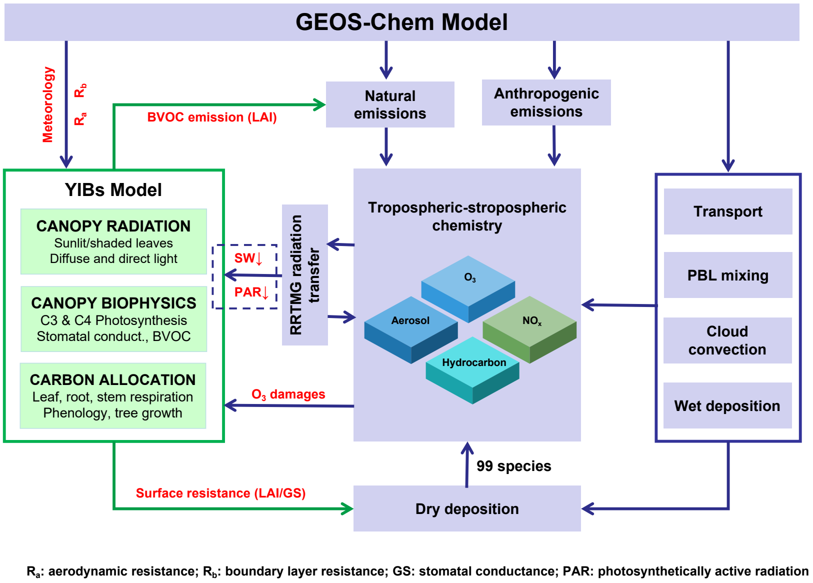

Figure 1 Diagram of the GC-YIBs global carbon-chemistry model. Processes with red fonts are implemented in this study. Processes with blue dashed box will be developed in the future.

Deleted: F

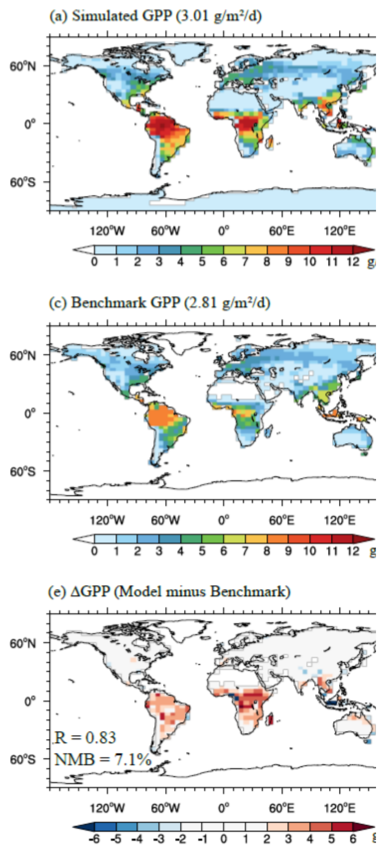

Deleted:

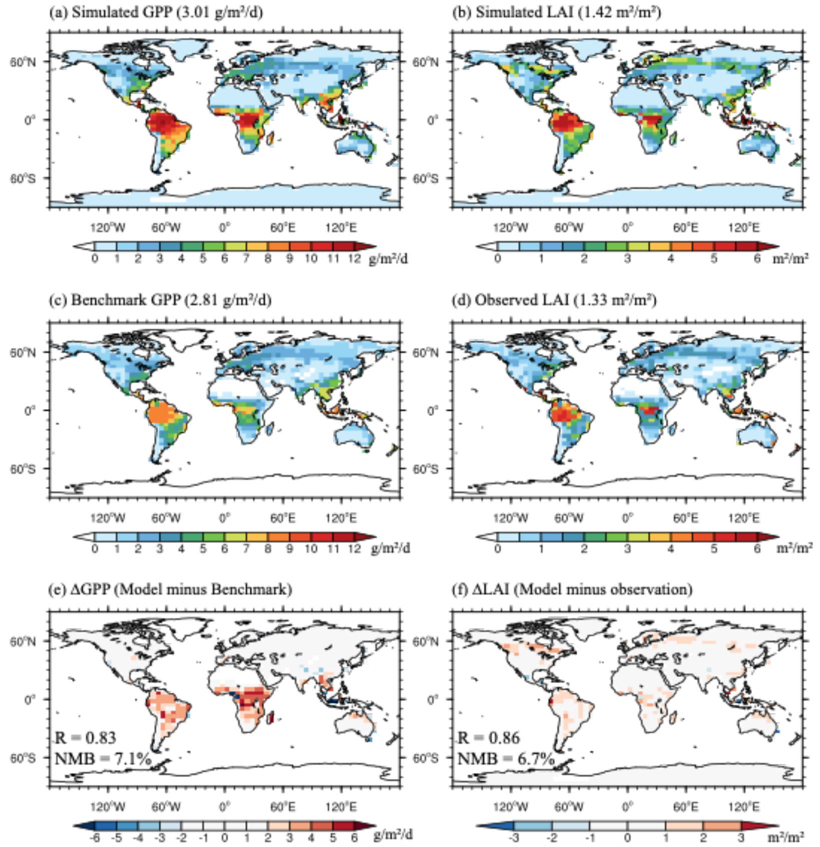

Figure 2 Annual gross primary productivity (GPP) and leaf area index (LAI) from Offline simulations **(a, b)**, observations **(c, d)**, and their differences **(e, f)** averaged for period of 2010-2012. Global area-weighted GPP and LAI are shown on the title brackets. The correlation coefficients (R) and global normalized mean biases (NMB) are shown in the bottom figures.

Formatted: Font:Bold

Formatted: Font:Bold

Formatted: Font:Bold

Deleted:

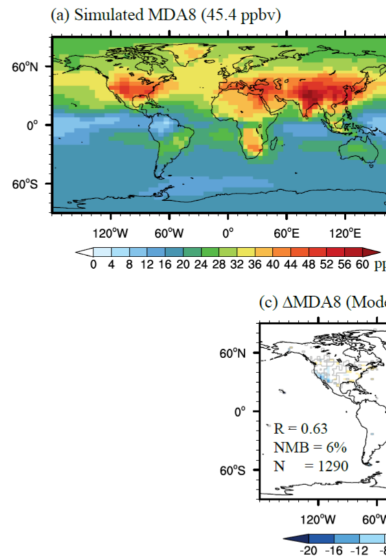

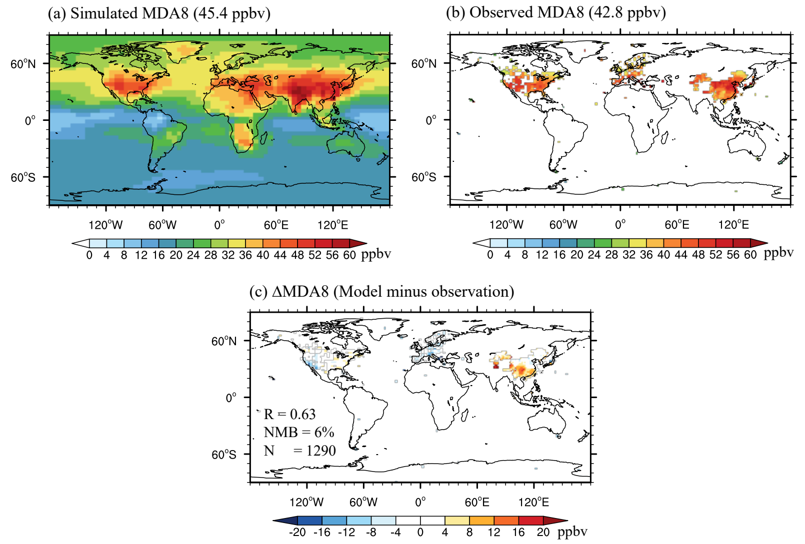

Figure 3 Annual surface O_3 concentrations ($[O_3]$) from Offline simulations **(a)**, observations **(b)**, and their differences **(c)** averaged for period of 2010-2012. Global area-weighted surface $[O_3]$ over grids with available observations are shown on the title brackets. The correlation coefficient (R) and global normalized mean biases (NMB) are shown in the bottom figures with indication of grid numbers (N) used for statistics.

Formatted: Font:Bold

Formatted: Font:Bold

Formatted: Font:Bold

Deleted:

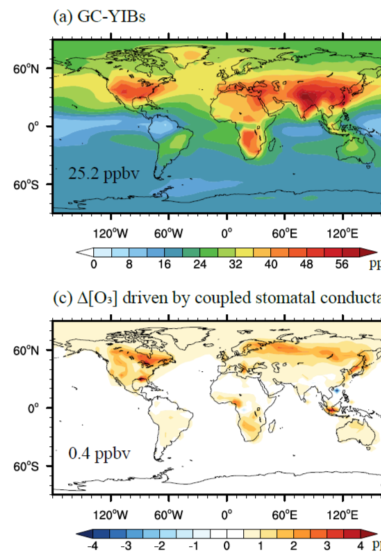

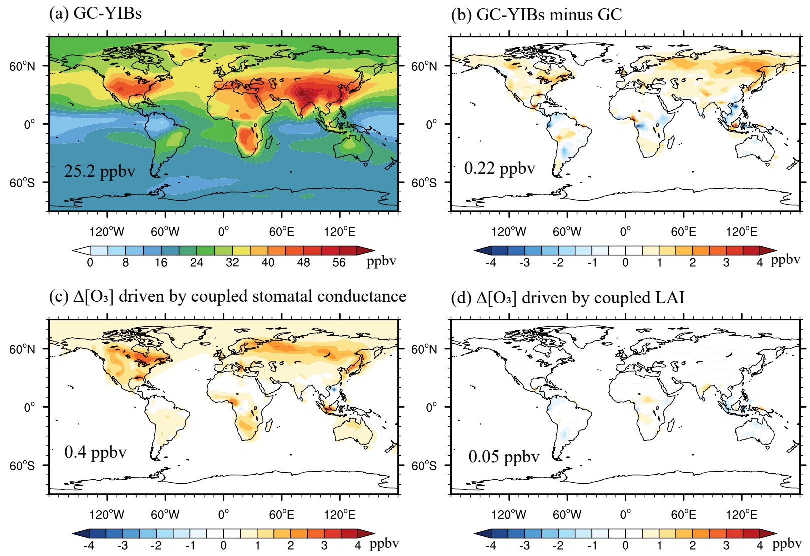

Figure 4 Simulated annual surface $[O_3]$ from online GC-YIBs model **(a)** and its changes (b-d) relative to Offline simulations. Changes of $[O_3]$ are caused by **(b)** jointly coupled LAI and stomatal conductance (Online_ALL – Offline), **(c)** coupled stomatal conductance alone (Online_ALL – Online_LAI), and **(d)** coupled LAI alone (Online_ALL – Online_GS). Global area-weighted $[O_3]$ or $\Delta[O_3]$ are shown in the figures.

Formatted: Font:Bold

Deleted: offline

Formatted: Font:Bold

Formatted: Font:Bold

Formatted: Font:Bold

Deleted:

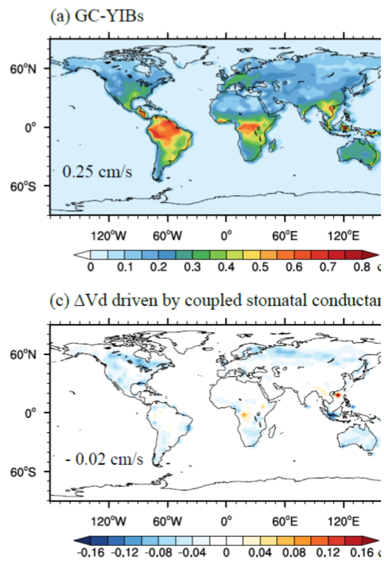

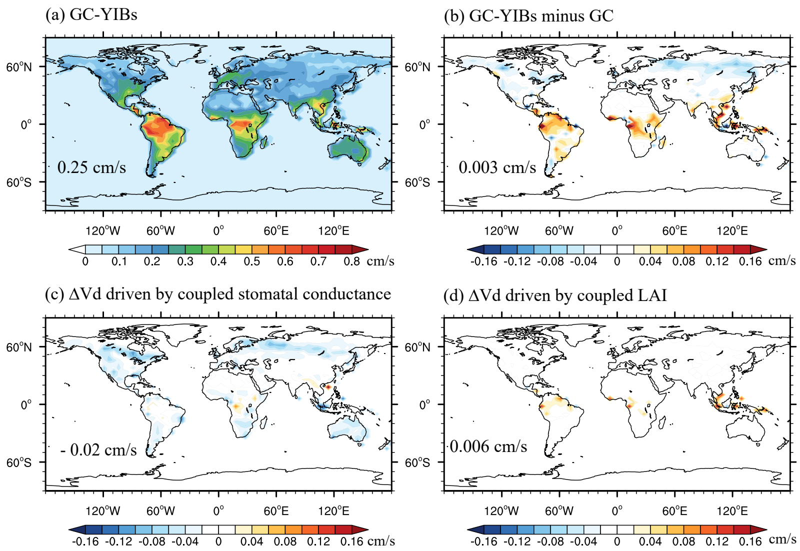

Figure 5 Simulated annual O_3 dry deposition velocity from online GC-YIBs model **(a)** and its changes caused by coupled LAI and stomatal conductance **(b-d)** averaged for period of 2010-2012. The changes of dry deposition velocity are driven by **(b)** coupled LAI and stomatal conductance (Online_ALL – Offline), **(c)** coupled stomatal conductance alone (Online_ALL – Online_LAI), and **(d)** coupled LAI alone (Online_ALL – Online_GS). Global area-weighted annual O_3 dry deposition velocity and changes are shown in the figures.

Formatted: Font:Bold

Formatted: Font:Bold

Formatted: Font:Bold

Formatted: Font:Bold

Formatted: Font:Bold

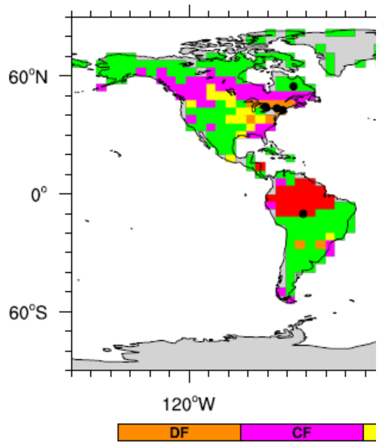

Deleted:

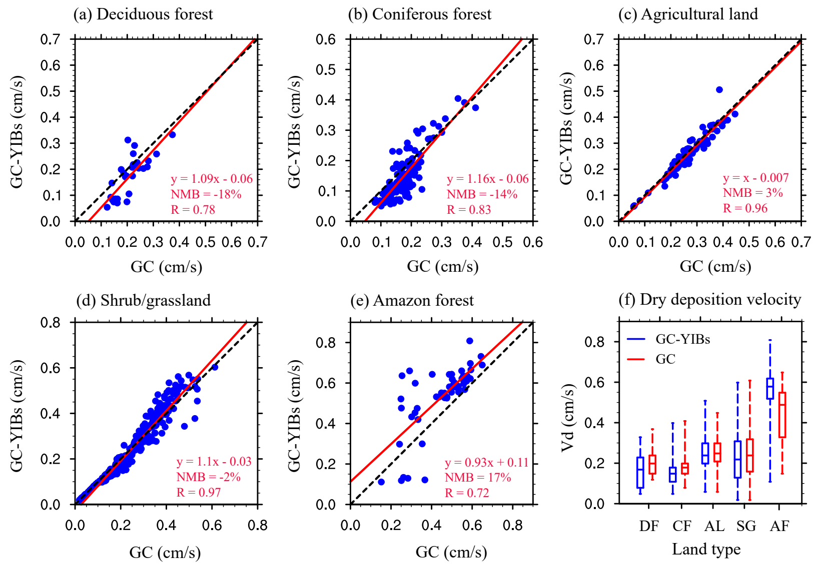

Figure 6 Comparisons of annual O_3 dry deposition velocity between online GC-YIBs (Online_ALL simulation) and GC (Offline simulation) models for different land types, including **(a)** Deciduous forest, **(b)** Coniferous forest, **(c)** Agricultural land, **(d)** Shrub/grassland, and **(e)** Amazon forest. The box plots of dry deposition velocity simulated by online GC-YIBs (blue) and GC models (red) for different land types are shown in **(f)**. Each point in (a)-(e) represents annual O_3 dry deposition velocity at one grid point averaged for period of 2010-2012. The red lines indicate linear regressions between predictions from GC-YIBs and GC models. The regression fit, correlation coefficient (R), and normalized mean biases (NMB) are shown on each panel.

Deleted: The major dry deposition type at each grid cell in GC model. Black dots indicate the locations of measurement sites used in evaluation (Table 2). DF, CF, AL, SG, AF represent deciduous forest, coniferous forest, agricultural land, shrub/grassland, and amazon forest, respectively. ... [79]

Deleted: and GC

Formatted: Font:Bold

Formatted: Font:Bold

Formatted: Font:Bold

Formatted: Font:Bold

Formatted: Font:Bold

Formatted: Font:Bold

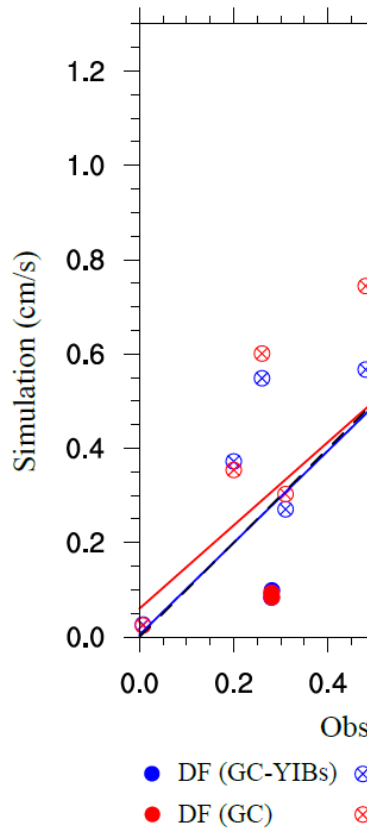

Deleted:

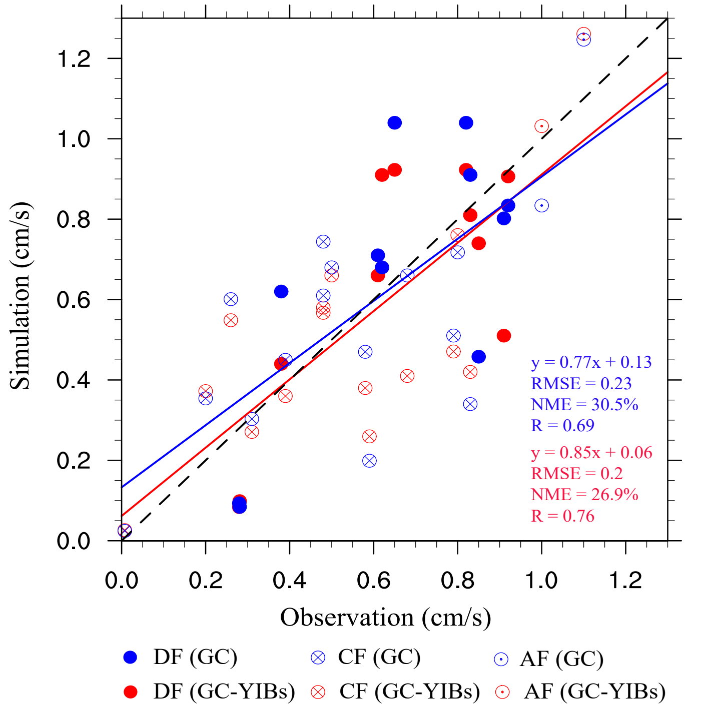

Figure 7 Comparison between observed and simulated O_3 dry deposition velocity at observational sites. The different marker types represent different land types. The blue and red markers represent the simulation results from online GC-YIBs (Online_ALL simulation) and GC (Offline simulation) models, respectively. The blue and red lines indicate linear regressions between simulations and observations. The regression fits, root-mean-square errors (RMSE), normalized mean errors (NME) and correlation coefficients (R) for GC-YIBs (blue) and GC (red) models are also shown.

Deleted: 8

Deleted:

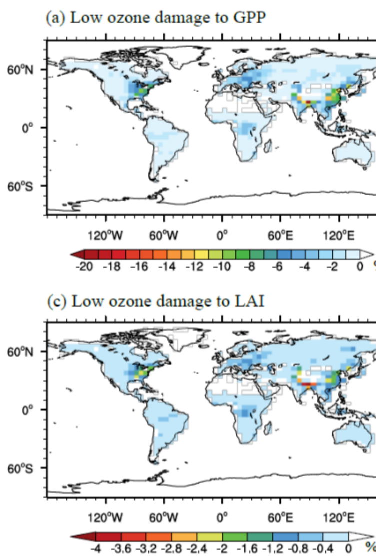

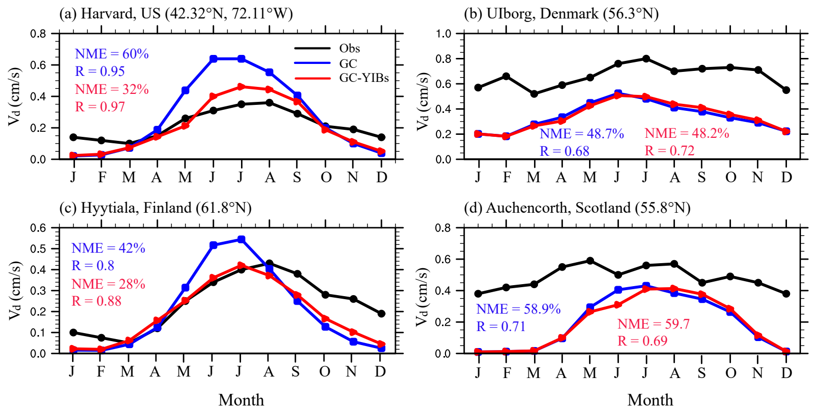

Figure 8 Comparison of monthly O_3 dry deposition velocity at Harvard **(a)**, Ulborg **(b)**, Hyytiala **(c)** and Auchencorth **(d)** sites. The black lines represent observed O_3 dry deposition velocity. The blue and red lines represent simulated O_3 dry deposition velocity from GC (Offline simulation) and online GC-YIBs (Online_ALL simulation) models, respectively.

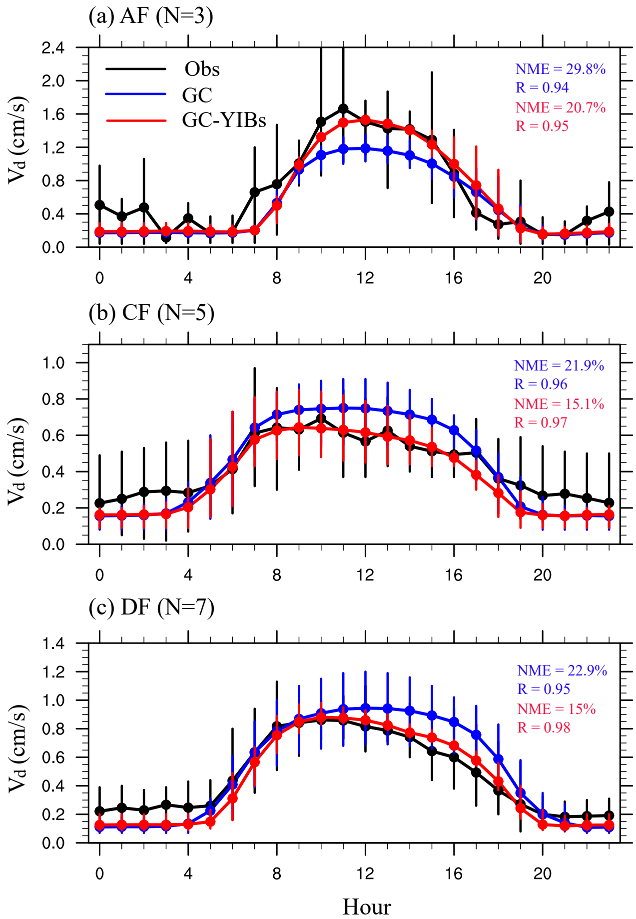

Figure 9 Comparison of multi-site mean diurnal cycle of O_3 dry deposition velocity at Amazon **(a)**, coniferous **(b)** and deciduous **(c)** forests. Errorbars represent the range of values from different sites. Black lines represent observed O_3 dry deposition velocity. The blue and red lines represent simulated O_3 dry deposition velocity by GC (Offline simulation) and online GC-YIBs (Online_ALL simulation) models, respectively. The site number (N), R, and NME are shown for each panel.

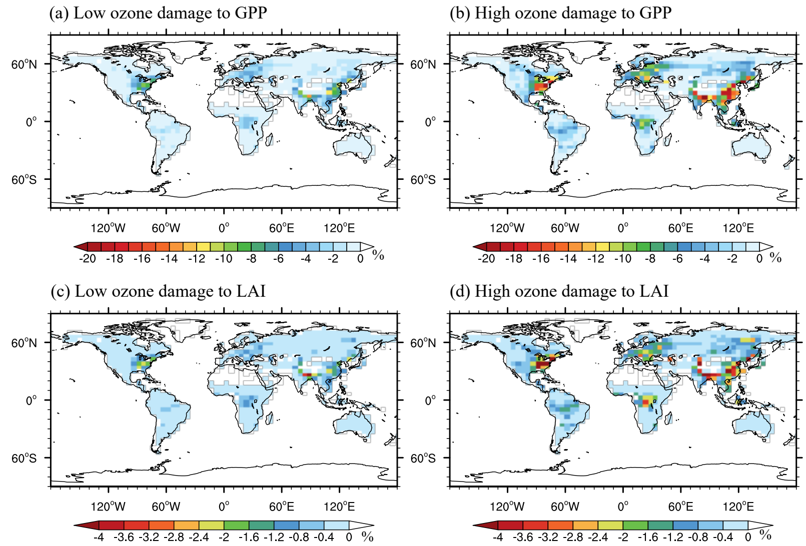

Figure 10 Percentage changes in **(a, b)** GPP and **(c, d)** LAI caused by O_3 damaging effects with **(a, c)** low (Online_ALL_LS simulation) and **(b, d)** high sensitivities (Online_ALL_HS simulation). Both changes of GPP and LAI are averaged for 2010–2012.

Formatted: Font:Bold

Formatted: Font:Bold

Formatted: Font:Bold

Deleted: .

Formatted: Font:Bold

Page 11: [1] Deleted	Xu Yue	1/19/20 6:11:00 PM

$$R_s = r_s \left\{ 1 + \frac{1}{\left[200(G+0.1)\right]^2} \right\} \left\{ \frac{400}{T_s(40 - T_s)} \right\} \frac{D_{H_2O}}{D_x} \quad (7)$$

Page 11: [2] Moved to page 13 (Move #1)	Xu Yue	1/19/20 6:11:00 PM

The Olson 2001 land cover map used in GC version 12.0.0 has a native resolution of 0.25°×0.25° and 74 land types (Olson et al., 2001). Each of the Olson land types is associated with a corresponding deposition land type with prescribed parameters. There are 74 Olson land types but only 11 deposition land types, suggesting that many of the Olson land types share the same deposition parameters. At specific grids (4°×5° or 2°×2.5°), dry deposition velocity is calculated as the weighted sum of native resolution (0.25°×0.25°).

Page 34: [3] Formatted	Xu Yue	1/19/20 6:11:00 PM

Font color: Auto

Page 34: [4] Formatted Table	Xu Yue	1/19/20 6:11:00 PM

Formatted Table

Page 34: [5] Formatted	Xu Yue	1/19/20 6:11:00 PM

Font color: Auto

Page 34: [6] Formatted	Xu Yue	1/19/20 6:11:00 PM

Font color: Auto

Page 34: [7] Formatted	Xu Yue	1/19/20 6:11:00 PM

Font color: Auto

Page 34: [8] Formatted	Xu Yue	1/19/20 6:11:00 PM

Font color: Auto

Page 34: [8] Formatted	Xu Yue	1/19/20 6:11:00 PM

Font color: Auto

Page 34: [8] Formatted	Xu Yue	1/19/20 6:11:00 PM

Font color: Auto

Page 34: [9] Formatted	Xu Yue	1/19/20 6:11:00 PM

Font color: Auto

Page 34: [10] Formatted	Xu Yue	1/19/20 6:11:00 PM

Font color: Auto

Page 34: [11] Merged Cells	Xu Yue	1/19/20 6:11:00 PM

Merged Cells

Page 34: [12] Formatted	**Xu Yue**	**1/19/20 6:11:00 PM**

Font color: Auto

Page 34: [13] Merged Cells	**Xu Yue**	**1/19/20 6:11:00 PM**

Merged Cells

Page 34: [14] Formatted	**Xu Yue**	**1/19/20 6:11:00 PM**

Font color: Auto

Page 34: [15] Formatted	**Xu Yue**	**1/19/20 6:11:00 PM**

Font color: Auto

Page 34: [16] Formatted	**Xu Yue**	**1/19/20 6:11:00 PM**

Font color: Auto

Page 34: [17] Formatted	**Xu Yue**	**1/19/20 6:11:00 PM**

Font color: Auto

Page 34: [18] Formatted	**Xu Yue**	**1/19/20 6:11:00 PM**

Font color: Auto

Page 34: [19] Formatted	**Xu Yue**	**1/19/20 6:11:00 PM**

Font color: Auto

Page 34: [20] Formatted	**Xu Yue**	**1/19/20 6:11:00 PM**

Font color: Auto

Page 34: [21] Formatted	**Xu Yue**	**1/19/20 6:11:00 PM**

Font color: Auto

Page 34: [22] Formatted	**Xu Yue**	**1/19/20 6:11:00 PM**

Font color: Auto

Page 34: [23] Formatted	**Xu Yue**	**1/19/20 6:11:00 PM**

Font color: Auto

Page 34: [24] Deleted	**Xu Yue**	**1/19/20 6:11:00 PM**

(

Page 34: [24] Deleted	**Xu Yue**	**1/19/20 6:11:00 PM**

(

Page 34: [25] Formatted	**Xu Yue**	**1/19/20 6:11:00 PM**

Font color: Auto

Page 34: [26] Formatted	**Xu Yue**	**1/19/20 6:11:00 PM**

Font color: Auto

Page 34: [27] Formatted	**Xu Yue**	**1/19/20 6:11:00 PM**

Font color: Auto

Page 34: [28] Formatted	**Xu Yue**	**1/19/20 6:11:00 PM**

Font color: Auto

Page 34: [29] Formatted	**Xu Yue**	**1/19/20 6:11:00 PM**

Font color: Auto

Page 34: [30] Formatted	Xu Yue	1/19/20 6:11:00 PM

Font color: Auto

Page 34: [31] Merged Cells	Xu Yue	1/19/20 6:11:00 PM

Merged Cells

Page 34: [32] Split Cells	Xu Yue	1/19/20 6:11:00 PM

Split Cells

Page 34: [33] Formatted	Xu Yue	1/19/20 6:11:00 PM

Font color: Auto

Page 34: [34] Formatted Table	Xu Yue	1/19/20 6:11:00 PM

Formatted Table

Page 34: [35] Formatted	Xu Yue	1/19/20 6:11:00 PM

Font color: Auto

Page 34: [36] Formatted	Xu Yue	1/19/20 6:11:00 PM

Font color: Auto

Page 34: [37] Formatted	Xu Yue	1/19/20 6:11:00 PM

Font color: Auto

Page 34: [38] Formatted	Xu Yue	1/19/20 6:11:00 PM

Font color: Auto

Page 34: [39] Formatted	Xu Yue	1/19/20 6:11:00 PM

Font color: Auto

Page 34: [40] Formatted	Xu Yue	1/19/20 6:11:00 PM

Font color: Auto

Page 34: [41] Formatted	Xu Yue	1/19/20 6:11:00 PM

Font color: Auto

Page 34: [42] Formatted	Xu Yue	1/19/20 6:11:00 PM

Font color: Auto

Page 34: [43] Formatted	Xu Yue	1/19/20 6:11:00 PM

Font color: Auto

Page 34: [44] Deleted	Xu Yue	1/19/20 6:11:00 PM

(

Page 34: [44] Deleted	Xu Yue	1/19/20 6:11:00 PM

(

Page 34: [45] Merged Cells	Xu Yue	1/19/20 6:11:00 PM

Merged Cells

Page 34: [46] Formatted	Xu Yue	1/19/20 6:11:00 PM

Font color: Auto

Page 34: [47] Formatted	Xu Yue	1/19/20 6:11:00 PM

Font color: Auto

Page 34: [48] Formatted	Xu Yue	1/19/20 6:11:00 PM

Font color: Auto

Page 34: [49] Formatted	Xu Yue	1/19/20 6:11:00 PM

Font color: Auto

Page 34: [50] Formatted	Xu Yue	1/19/20 6:11:00 PM

Font color: Auto

Page 34: [51] Formatted	Xu Yue	1/19/20 6:11:00 PM

Font color: Auto

Page 34: [52] Formatted	Xu Yue	1/19/20 6:11:00 PM

Font color: Auto

Page 34: [53] Formatted	Xu Yue	1/19/20 6:11:00 PM

Font color: Auto

Page 34: [54] Formatted	Xu Yue	1/19/20 6:11:00 PM

Font color: Auto

Page 34: [55] Formatted	Xu Yue	1/19/20 6:11:00 PM

Font color: Auto

Page 34: [56] Deleted	Xu Yue	1/19/20 6:11:00 PM

(

Page 34: [56] Deleted	Xu Yue	1/19/20 6:11:00 PM

(

Page 34: [57] Merged Cells	Xu Yue	1/19/20 6:11:00 PM

Merged Cells

Page 34: [58] Formatted	Xu Yue	1/19/20 6:11:00 PM

Font color: Auto

Page 34: [59] Merged Cells	Xu Yue	1/19/20 6:11:00 PM

Merged Cells

Page 34: [60] Formatted	Xu Yue	1/19/20 6:11:00 PM

Font color: Auto

Page 34: [61] Formatted	Xu Yue	1/19/20 6:11:00 PM

Font color: Auto

Page 34: [62] Formatted	Xu Yue	1/19/20 6:11:00 PM

Font color: Auto

Page 34: [63] Formatted	Xu Yue	1/19/20 6:11:00 PM

Font color: Auto

Page 34: [64] Formatted	Xu Yue	1/19/20 6:11:00 PM

Font color: Auto

Page 34: [65] Formatted	**Xu Yue**	**1/19/20 6:11:00 PM**

Font color: Auto

Page 34: [66] Formatted	**Xu Yue**	**1/19/20 6:11:00 PM**

Font color: Auto

Page 34: [67] Formatted	**Xu Yue**	**1/19/20 6:11:00 PM**

Font color: Auto

Page 34: [68] Formatted	**Xu Yue**	**1/19/20 6:11:00 PM**

Font color: Auto

Page 34: [69] Formatted	**Xu Yue**	**1/19/20 6:11:00 PM**

Font color: Auto

Page 34: [70] Formatted	**Xu Yue**	**1/19/20 6:11:00 PM**

Font color: Auto

Page 34: [71] Formatted	**Xu Yue**	**1/19/20 6:11:00 PM**

Font color: Auto

Page 34: [72] Formatted	**Xu Yue**	**1/19/20 6:11:00 PM**

Font color: Auto

Page 34: [73] Formatted	**Xu Yue**	**1/19/20 6:11:00 PM**

Font color: Auto

Page 34: [74] Deleted	**Xu Yue**	**1/19/20 6:11:00 PM**

(

Page 34: [74] Deleted	**Xu Yue**	**1/19/20 6:11:00 PM**

(

Page 34: [75] Formatted	**Xu Yue**	**1/19/20 6:11:00 PM**

Font color: Auto

Page 34: [76] Formatted	**Xu Yue**	**1/19/20 6:11:00 PM**

Font color: Auto

Page 34: [77] Formatted	**Xu Yue**	**1/19/20 6:11:00 PM**

Font color: Auto

Page 34: [78] Formatted	**Xu Yue**	**1/19/20 6:11:00 PM**

Font color: Auto

Page 40: [79] Deleted	**Xu Yue**	**1/19/20 6:11:00 PM**

The major dry deposition type at each grid cell in GC model. Black dots indicate the locations of measurement sites used in evaluation (Table 2). DF, CF, AL, SG, AF represent deciduous forest, coniferous forest, agricultural land, shrub/grassland, and amazon forest, respectively.

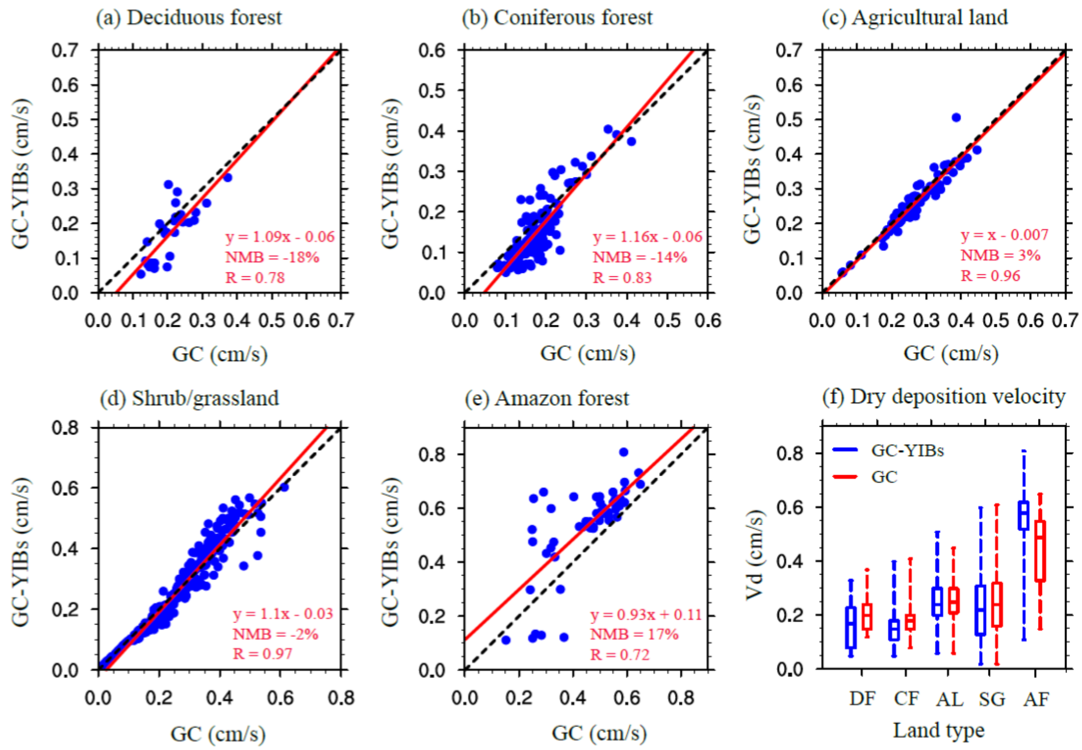

(a) Deciduous forest
GC-YIBs (cm/s)
GC (cm/s)
y = 1.09x - 0.06
NMB = -18%
R = 0.78
(b) Coniferous forest
GC-YIBs (cm/s)
GC (cm/s)
y = 1.16x - 0.06
NMB = -14%
R = 0.83
(c) Agricultural land
GC-YIBs (cm/s)
GC (cm/s)
y = x - 0.007
NMB = 3%
R = 0.96
(d) Shrub/grassland
GC-YIBs (cm/s)
GC (cm/s)
y = 1.1x - 0.03
NMB = -2%
R = 0.97
(e) Amazon forest
GC-YIBs (cm/s)
GC (cm/s)
y = 0.93x + 0.11
NMB = 17%
R = 0.72
(f) Dry deposition velocity
GC-YIBs
GC
Vd (cm/s)
DF CF AL SG AF
Land type

Figure 7